

Characterization of drivers' heterogeneity and its integration within traffic simulation

Anesiadou^b, A., Makridis^a, M., Mattas^b, K., Fontaras^b, G., Ciuffo^{b,1}, B.

^aETH Zürich, Institute for Transport Planning and Systems (IVT), Zürich, CH

^bEuropean Commission – Joint Research Centre., Ispra (VA), Italy

Abstract

Drivers' heterogeneity and the broad range of vehicle characteristics are considered primarily responsible for the stochasticity observed in road traffic dynamics. Assessing the differences in driving style and incorporating individual driving behaviour in microsimulation has attracted significant attention lately. The first topic is studied extensively in the literature. The second one, on the contrary, remains an open issue. The present study proposes a methodology to characterise driving style in the free-flow regime and to incorporate drivers' heterogeneity within a microsimulation framework.

The methodology uses explicit and simplified modelling of the vehicle powertrain to separate the drivers' behavior from the vehicle characteristics. In this light this study proposes a novel metric called Independent Driving Style (*ids*) that is independent of the vehicle dynamics and uncorrelated with the specific vehicle speed. Data collected from an experimental campaign involving 20 drivers demonstrate the robustness of the proposed framework.

Results show that inter and intra-driver heterogeneity can be captured by log-normal distributions of the *ids*. Drivers are classified into three different groups (dynamic, ordinary and timid drivers). Differences in the behaviour of different drivers are more prominent in specific moments rather than when observing them from an overall perspective. Finally, derived driver distributions are used to reproduce the detected driving behavior in a microsimulation environment in a stochastic way. Simulations are assessed from a macro and micro level, where in both cases, a good fit is found between simulated and observed results.

Combined with information on the vehicle fleet composition, the proposed approach thus represents a promising framework to characterize and simulate the effect of driver heterogeneity with potentially significant benefits for the reliability of traffic simulations.

1 Introduction

In the years to come, drastic changes in the vehicles' behaviour will start to appear faster than ever before, fostered by new driving assistance and automation systems, affecting traffic flow dynamics in road transport networks. Technological innovation affects several dimensions of road transport, including the infrastructure (physical and digital) and different in-vehicle systems (e.g. powertrain, sensors, control logic, etc.). In combination with that, increasing population, traffic demand, high congestion, air pollution and road safety are factors challenging the management of future road transport systems.

In order to understand the impact of new technologies on traffic dynamics and properly design future traffic management approaches, comprehensive traffic simulation models will need to be derived. In particular, differently from the past, driving behaviour will be one of the main variable among different traffic scenarios and therefore future models will need to properly handle its heterogeneity into account.

¹ Corresponding author. E-mail: Biagio.CIUFFO@ec.europa.eu

Unfortunately traditional traffic models considering the driver-vehicle system as a single entity. In particular, traditional models define the behaviour of the vehicle-driver system without differentiation between what can be attributed to vehicle characteristics (powertrain, shape, acceleration capabilities etc.) and what is instead related to driver attitudes (aggressiveness levels). This makes it difficult to characterise the heterogeneity in longitudinal driving behaviour, which has a significant impact on the stochasticity observed under heavy traffic (Huang et al., 2018; Ossen and Hoogendoorn, 2011). The situation is further complicated by the advent of automation and Advanced Driver Assistance Systems (ADAS) and the need to understand the differences in the behaviour of human drivers (Calvert and van Arem, 2020; Zhao et al., 2020) to study the potential effect of new technologies on road transport (Makridis et al. 2020c, Makridis et al. 2020d).

Given the limitation of existing car-following models, driving heterogeneity is often simulated in a stochastic way, without specific connections with any physical mechanism (Laval et al., 2014; Treiber and Kesting, 2013).

Some models have started to explicitly consider the impact of vehicle dynamics on longitudinal driving behaviour in recent years, establishing a direct link with vehicles' technical specifications (Fadhoun and Rakha, 2020; Makridis et al., 2019; Rakha et al., 2004, 2012). Their results reveal that a better reproduction of the variability in the driving behaviours and the vehicle dynamics can improve accuracy in microsimulation scenarios (Ciuffo et al., 2018; Fadhoun and Rakha, 2020; He et al., 2020; Rakha et al., 2012). Makridis et al. (Makridis et al., 2020a, Makridis et al., 2020b) have shown that the explicit simulation of the powertrain system can explain at least part of traffic heterogeneity, calling for new studies to cover the remaining part, namely that related to the explicit simulation of the drivers' attitudes.

Researchers have already invested efforts in analysing the behaviour of drivers and mentioned the connection between variability in the driving behaviour and several traffic-related phenomena such as traffic oscillations, capacity drop, hysteresis, and stop and go waves (Chen et al., 2014; Huang et al., 2018; Laval and Leclercq, 2010; Saifuzzaman et al., 2017; Zheng et al., 2011). When referring to the fundamental diagram, Kessels (Kessels, 2019) mentions that a wide scatter is observed in the density-flow plots due to the variability in vehicle characteristics and driver behaviour. With the recent technological advances in communications and data acquisition devices, conduction of large experimental campaigns and acquisition of massive trajectory data is possible, allowing the study of the vehicle-driver system in more detail.

Different kinds of studies use actual driving data, focusing more on identifying risky/unsafe/aggressive drivers (Eboli et al., 2016; Feng et al., 2017; Lee and Jang, 2019). Such approaches are mostly related to traffic safety. Others are mostly related to behavioural analysis; Li et al 2017 (Li et al., 2017) used manoeuvre transition probabilities to estimate driving style, and they finally classified drivers into three groups based on how risky the driver is. From an engineering perspective, Wang et al 2017 (Wang et al., 2017) used a Bayesian method on naturalistic driving data to assign each driver to a frequency distribution of driving patterns and compared them through Kullback-Leibler divergence. Their approach does not take into account the different dynamics, which refer to different speed levels. Qi et al 2019 (Qi et al., 2019) overcame this weakness and characterised drivers in relation to different driving speed conditions using acceleration, speed difference and time gap measurements. Finally, each driver is characterised by different driving styles with different probabilities. The different driving conditions were limited to five-speed clusters, reaching a maximum speed of approximately 15 m/s. Such approaches do not account for the vehicle characteristics, as the analysis still focuses on the driver-vehicle system as a whole. In a recent, extensive study, a driving style metric is proposed based on the deviation of joint speed-acceleration distributions of measured data from a real-world fleet sample (Tanvir, 2018). However, the driving style metric used in this approach is not separating the driver from the vehicle. The abovementioned studies are not directly applicable to support microsimulation frameworks.

Driver heterogeneity has also been studied by analysing the values of different car-following models' parameters calibrated on real-world trajectory data. For example, Ossen and Hoogendoorn (Ossen and Hoogendoorn, 2011) used experimental data and calibrated eight different CF models considering that each of them expresses a different driving style. They differentiated between trucks and passenger cars and studied inter-driver heterogeneity based on the argumentation that different CF models better represented certain groups of drivers. Furthermore, the intra-driver heterogeneity was investigated by checking the spread in empirical distributions of the estimated parameters of a specific group of drivers. Taylor et al 2015 (Taylor et al., 2015) calibrated Newell's extension model with time-varying parameters to observe intra driver heterogeneity. Similar research was conducted by Zhu et al 2018 (Zhu et al., 2018). Finally, James and Hammit (James and Hammit, 2019) calibrated three CF models per driver from naturalistic data and concluded that clusters of similar driving behaviours are assigned to different driver attributes. The studies mentioned above contributed to shed light on different aspects of driving/traffic heterogeneity. However, their results are linked to the specific CF models. Additionally, the following issues are identified by the authors: i) Calibrated and observed model parameters do not always numerically coincide (Zhu et al., 2018), hence they do not reflect actual drivers' characteristics and their values may be affected by model overfitting. ii) Car-following models consider the driving-vehicle system as a single entity, and therefore, parameters' values do not necessarily represent driving attitudes. iii) the calibration problem is non-trivial, and the use of an improper framework can significantly affect the robustness of the achieved results and conclusions (Punzo et al., 2012).

When only referring to driver style reproduction, Javanmardi et al. (Javanmardi et al., 2017) constructed a driver model to represent three different driving styles for fuel consumption. Xu et al. (Xu et al., 2015) introduced a style-oriented driver model to reproduce the original human driving behaviour and potentially contribute to robot driver development. Both approaches propose control-based driving style models that can reproduce individual trajectories, but they do not consider traffic dynamics and intra-driver behaviour variability.

Most of the research papers investigated, are either not applicable to traffic simulation frameworks (no quantitative outputs) or linked explicitly to existing car-following models without formal distinction between the driver and the vehicle. A recent study concludes that the next challenge in traffic simulation is incorporating driver heterogeneity in simulation models (Itkonen et al., 2020). To fill this gap, the authors argue that the vehicle-driver system can be studied, simulated, calibrated and validated separately, paving the way to new findings that are not bounded by the intrinsic differences between the two sub-systems. Furthermore, it should be noted that the vehicle powertrain is a constant source of power for all the drivers that may drive this vehicle. Consequently, vehicles can be more easily clustered based on their different dynamics in a relatively small, fixed set. This separation will highlight the variation among the behaviours of the drivers, which can be investigated separately.

Learning from the limitations identified from the literature, the approach adopted in the present study presents:

- A methodology to study the driver independently from the vehicle and derive driver style probability density functions
- Application of this methodology to experimental results
- Showcase the potentials of incorporating the derived driver-characteristic functions in a vehicle dynamics based microsimulation framework

In this context, the present paper presents a quantitative driving style metric and a mathematical formulation to incorporate it in a microsimulation framework. In particular, the Independent Driving Style (*ids*) metric is first proposed. Then it is used to characterise the driving style of 20 drivers involved in a dedicated test

campaign. Finally, it is used combined with the Microsimulation Free-flow acceleration model (MFC) (Makridis et al., 2019) to simulate acceleration patterns in a traffic simulation framework.

The remainder of the paper is organised as follows. Firstly, the literature background is presented. Secondly, the methodology is explained, followed by the description of the case study. Afterwards, the results section is introduced, and finally, the conclusion, limitations and future work are presented.

2 Methodology

We propose a methodological approach for driver heterogeneity characterisation and driving behavior reproduction in microsimulation. A schematic representation is illustrated in Figure 1.

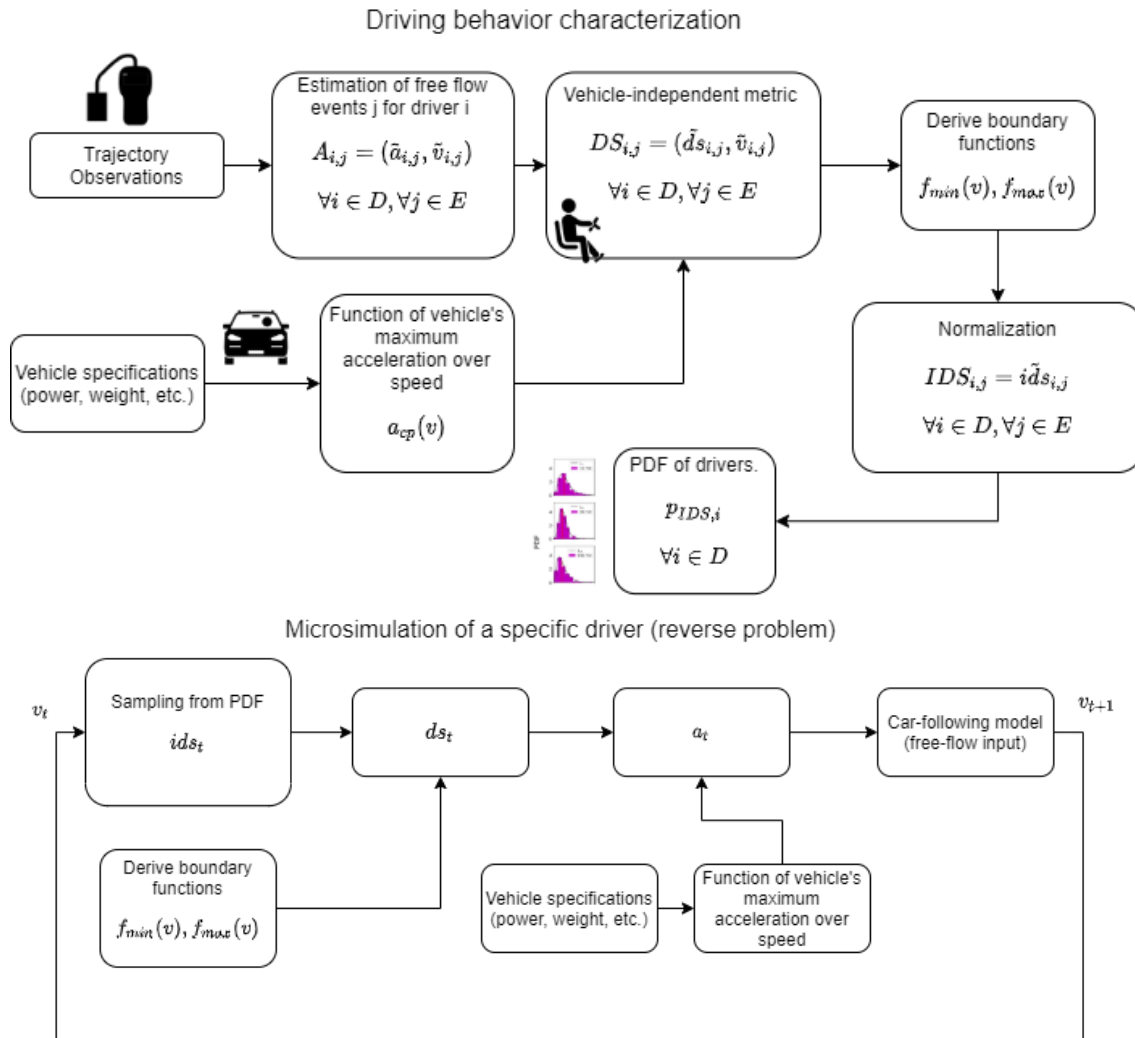


Figure 1. Schematic representation of the proposed methodological approach for driving behavior characterisation and reproduction of an observed driver in microsimulation.

The methodology uses vehicle trajectory data to isolate free flow acceleration events which are considered the most representative phases to characterize driving behavior. In fact differences among drivers are clearer the driver's behaviour is not constrained by obstacles such as another vehicle in front, a traffic light, etc.

The characteristics of the vehicle powertrain are then filtered out using a novel driving style metric that considers the amount of available engine power the driver uses while driving. In other words, rather than using vehicle speed and acceleration that are also function of the vehicle capabilities, taking into account the available engine power is considered a clearer metric to characterize vehicle behavior. More details will be provided in the following sections.

Finally, using the proposed driving style metric the simulation of the observed driver behaviours in a microsimulation environment (reverse problem) is carried out. It is worth underlining that the new metric does not associate a single value to each driver but a whole distribution from which the instantaneous value can be sampled. This is crucial in order to include the effect of the driving style variability due to, e.g. fatigue, traffic and weather conditions, etc.

2.1 Estimation of free flow conditions from vehicle trajectories

As already mentioned, the primary assumption of the proposed methodology is that individual driving behaviours are particularly visible under free-flow conditions when the drivers are not constrained by other vehicles, obstacles, and other elements downstream. For this reason, from a database of vehicle trajectories, acceleration events are isolated by considering sufficiently long speed increases that can be compatible with the fact that the driver was not constrained in its motion.

In particular, acceleration events are selected on the basis of the following considerations: a) during car-following, usually the vehicles do not continuously accelerate for an extended period (time parameter w); b) during a typical car-following acceleration event, the speed difference between the start and end speed cannot exceed a certain threshold (speed parameter Δv_{th}). The acceleration events are detected as partial trajectories sufficiently long (w) for a vehicle to have a noteworthy positive speed difference (Δv_{th}) from a starting (local minimum) to an ending (local maximum) speed, assuming that at this time, the driver accelerates freely up to the desired speed.

At first, a heuristic algorithm is implemented on the speed series to identify all the acceleration events for all the drivers within a dataset. Local minima and local maxima constitute the beginning and ending speeds of the acceleration events. Time instances with acceleration values smaller than 0.01 m/s^2 have been excluded.

Secondly, a car-following experiment (He et al., 2020; Makridis et al., 2021) with a platoon of five vehicles was used as ground truth to estimate the second parameter value Δv_{th} . The goal is to identify plausible heuristic thresholds for Δv_{th} that distinguish free flow with following conditions. To achieve that, we define a time window w and the following indicator applied at all speed series of each following vehicle:

$$\begin{aligned} \Delta v_{i,t} &= v_{i,t} - v_{i,t-w} \quad \forall t \in [w, t_{max}] \quad \forall i \in [2, 5] \text{ with } i \text{ being the following vehicle} \\ \Delta v_w &= \Delta v_{t_{75}} \end{aligned} \tag{1}$$

where $\Delta v_{t_{75}}$ is the 75th percentile of the Δv_t and Δv_t is consisted of all the $\Delta v_{i,t}$ values.

Figure 2 illustrates the histograms referring to the recorded Δv_t values for four different time windows w . The Δv_w is mentioned in each histogram plot as the threshold value Δv_{th} defining the border between free-flow and car-following conditions.

To summarise, to identify an acceleration event as free-flow, firstly, its time duration was checked (Δt), and the event was assigned to one of the four respective time windows. Events with duration lying within [2, 7) or [7, 12) or [12, 17) seconds were assigned to the 1st, 2nd or 3rd time window, respectively. Events with a

duration longer than 17 secs, were assigned to the 4th window. At a second step, if the events Δv_w value is larger than the threshold defined in Eq. 1, the event would then be considered to be in free-flow conditions.

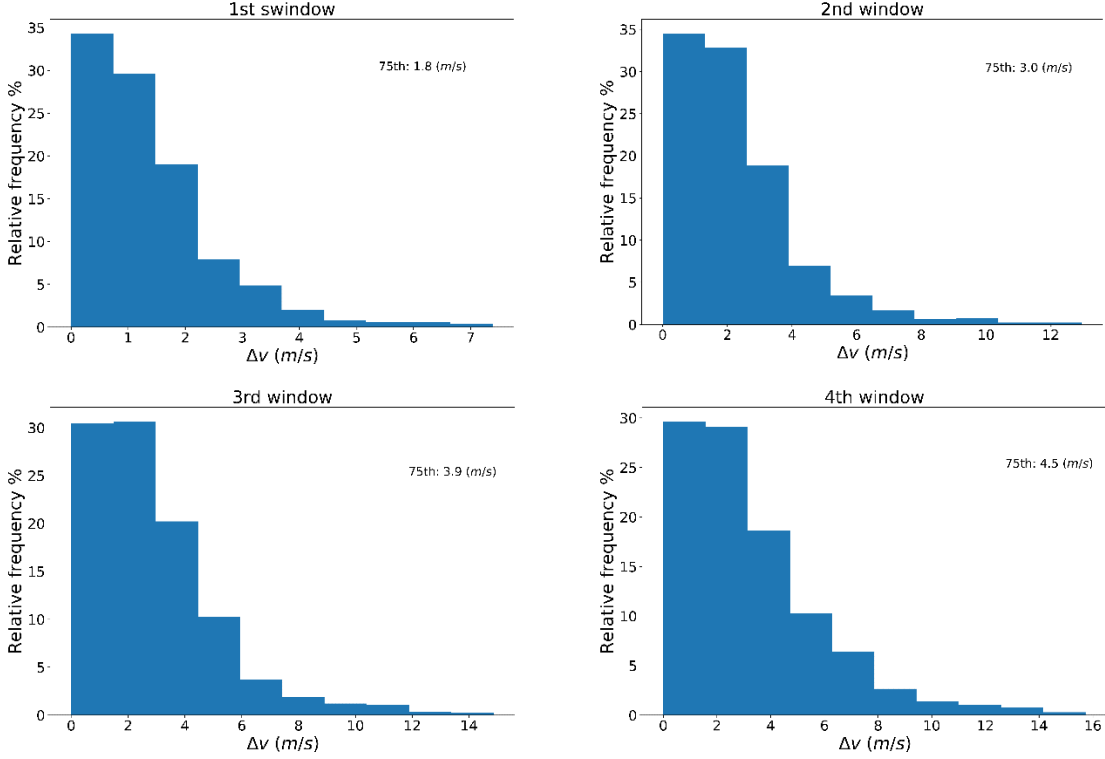


Figure 2. Histograms of speed difference of CF experiments regarding four different time windows which serve as thresholds for the identification of free flow acceleration events.

Although each of the detected events corresponds to the same driver, we assume that each event demonstrates a different behaviour (inter-drive heterogeneity). This is a reasonable assumption since a driver can produce different patterns. Finally, the detected events are represented by the median values of acceleration and speed. Figure 3 illustrates the detection of acceleration events for a given speed profile. Only values between the 10th and 90th percentile of each event are considered, as the driver behaviour is different near the beginning and the end of the acceleration (Makridis et al., 2019).

Thus, we have a dataset of drivers, where each driver is expressed with i where $i \in D$ and D is the set of all available drivers. In each driver's trajectory, we detect partial trajectories (i.e. events) $j \in E_i$ and E_i is the set of all events for a given driver. Each event $A_{i,j}$ then is characterised by only two values, the median acceleration and the median speed during this trajectory:

$$A_{i,j} = (\tilde{a}_{i,j}, \tilde{v}_{i,j}) \quad (2)$$

where i is the driver, j is the event id and $\tilde{a}_{i,j}, \tilde{v}_{i,j}$ are the respectively median acceleration and speed values of the event.

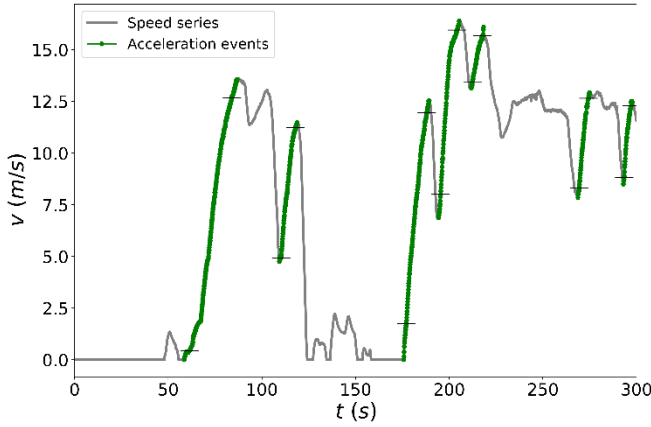


Figure 3. Example of acceleration events from measured speed profiles.

2.2 Introduction of Independent Driving Style metric

The main idea is to characterise a driver with a metric that at first is independent of the power capabilities of the vehicle and secondly reliable enough to provide a comparative analysis between two drivers independently of the traffic conditions.

Assuming that the specifications of the vehicle are known, the maximum possible acceleration as a function of speed and gear can be calculated using a vehicle dynamics model. There are several models of this type in the literature (Fadhoun and Rakha, 2020; Makridis et al., 2019; Rakha et al., 2004, 2012). Here we use the one proposed in Makridis et al. (2019).

Let $a_{cp}(g, v(t))$ be this maximum acceleration (in the following notation, we omit time for simplicity, i.e. $a_{cp}(g, v_t)$), where v_t is a speed measurement at time instance t . The function $a_{cp}(g, v_t)$ is used to normalise the acceleration observation based on the vehicle's power capabilities. Concretely, the following vehicle-free quantity is introduced:

$$ds_t = \frac{a_t}{a_{cp}(g, v_t)} \quad (3)$$

where a_t and v_t are the measured speed and acceleration of the vehicle at time t , g is the gear employed at time t and $a_{cp}(v_t)$ is the maximum possible vehicle's acceleration for the given speed v_t . The ds_t value lies within the range of (0,1], since the driver cannot impose an acceleration higher than the maximum acceleration the car can deliver for the given speed. Conceptually, values close to 0 denote timid drivers, while values close to 1 dynamic drivers, tending to bring the vehicle close to its limits.

Using the relation defined in Eq. 3, we can substitute the median acceleration term in Eq.2 for each event with its corresponding ds values, and similarly to Eq. 2 we revise the acceleration event:

$$DS_{i,j} = (\tilde{ds}_{i,j}, \tilde{v}_{i,j}) \quad (4)$$

where j is the event id and i the driver, $\tilde{ds}_{i,j}$ is the median ds_t value and $\tilde{v}_{i,j}$ is the median v_t speed.

It should be noted that observed accelerations are not uniform across the entire speed range of the vehicle. This is expected since vehicles have enough power to deliver high accelerations at low speeds but not at higher ones. An illustrative example is shown in Figure 4 (a) that presents \tilde{a}_j over \tilde{v}_j for all drivers and it is possible to notice that the distribution is not uniform and \tilde{a}_j values show a decreasing pattern with increasing

speed. In this figure, one can also notice that the data are quantised due to the logging frequency and precision of the measurement. Figure 4 (b) presents \widetilde{ds}_j over \widetilde{v}_j for all drivers and it is obvious that \widetilde{ds}_j is positively correlated with speed. This means that at lower speeds, most drivers have small accelerations compared to the maximum vehicle acceleration at that speed. It can be argued that comfort is the factor that limits acceleration. On the contrary, as the speed increases, the driver needs to use more of the vehicle's acceleration potential to achieve the desired speed.

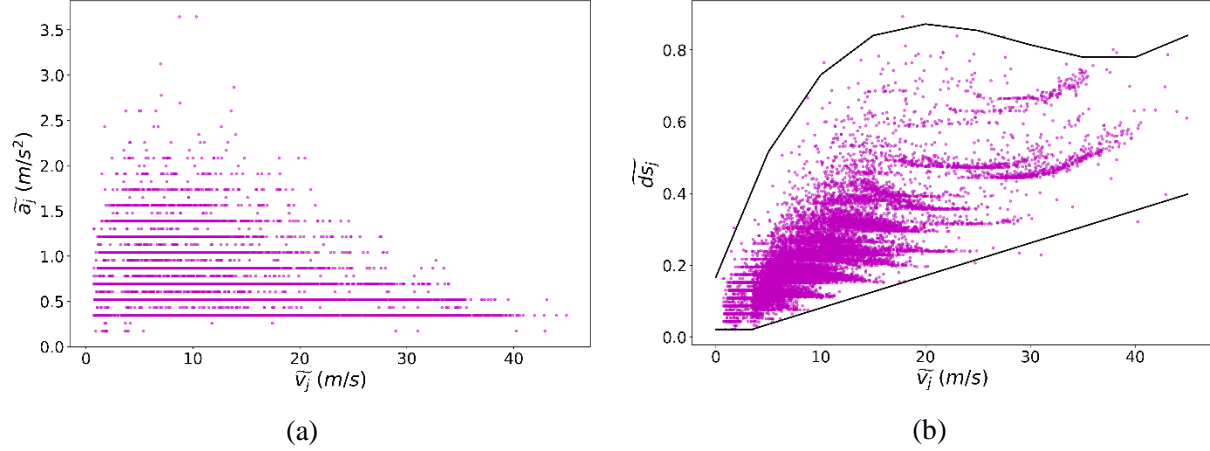


Figure 4. a) Median acceleration per event versus median speed per event plot, b) Median ds per event versus median speed per event plot.

This correlation creates a bias, since the empirical campaigns are hardly ever balanced in terms of measured speed ranges, and this brings us to the second goal. The proposed methodology introduces a new quantity that is derived from \widetilde{ds}_j aiming to eliminate the correlation on speed. There may be many vehicles with different specifications and, therefore, different levels of correlation between the metric and the speed.

It is assumed that the sample of empirical measurements is enough to characterise any possible driver. This is a hard assumption, which however, can be easily updated as the database of the empirical measurements grows. Thus, we create an operational domain for the $DS_{i,j}$ events, bounded by the black-colored curves, namely $f_{min}(\widetilde{v})$ and $f_{max}(\widetilde{v})$ in Figure 4 (b). Those curves are defined using polynomial fitting. The characteristics of the fitted polynomials are mentioned in Appendix A, to facilitate the reproduction of the methodology. Subsequently, the following normalised vehicle-free quantity, referred to as Independent normalised Driving Style metric is established as:

$$ids_j = \frac{\widetilde{ds}_j - f_{min}(\widetilde{v})}{f_{max}(\widetilde{v}) - f_{min}(\widetilde{v})} \quad (5)$$

where, ds_t corresponds to the vehicle-free metric defined in Eq.3, $f_{min}(\widetilde{v})$ and $f_{max}(\widetilde{v})$ are the polynomial functions that enclose the space for the $DS_{i,j}$ events. Some outliers have been left outside the f curves. In general, this can be parametrised depending on the noise of the experimental data.

Using the relation defined in Eq.5, we can assume that the developed metric is independent of the speed and therefore the events can be now described by ids alone:

$$IDS_{i,j} = ids_{i,j} \quad (6)$$

where j is the event id and i the driver, $ids_{i,j}$ is the ids value referring to the event of each driver.

The metric ids is a metric normalised to the driving domain of the database and can take values in the range $[0, 1]$. Values approaching 1 indicate a driver that for the specific event is located in the upper bound of the driving domain in Figure 4 (b) and therefore has higher ds_j values with respect to other drivers, which

means that it has exploited more the acceleration potential of the vehicle. For the whole $IDS_{i,j}$ events dataset, ids_j are plotted over \tilde{v}_j for all drivers in Figure 5, and as can be seen, this metric shows no specific pattern or correlation with speed. More details on the correlation between ids_j with \tilde{v}_j are presented in Appendix B.

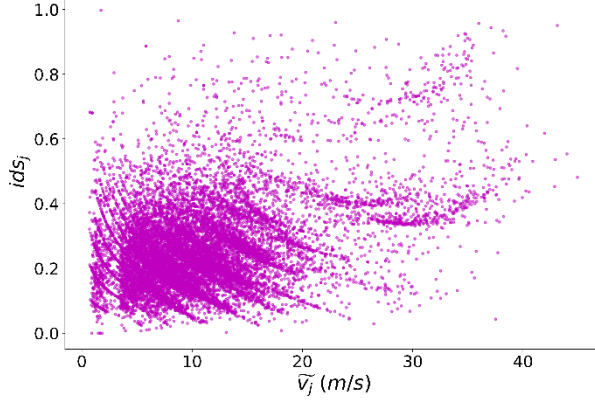


Figure 5. ids per event versus median speed per event for all drivers.

2.3 Inferring continuous probability density functions from discrete variables

At this stage, $IDS_{i,j}$ events (discrete variables) are represented with probability mass functions (PMF) of empirical distributions for each driver i . Afterwards, we assume a log-normal probability density function (PDF), which we fit on the PMF in order to obtain its continuous representation.

By fitting a well-known distribution $p_{IDS,i}$ on the $IDS_{i,j}$ events of each driver, we can enable analytical comparisons or even exploit it to reproduce the driving behavior in microsimulation. Each fitted PDF $p_{IDS,i}$ for a given driver i can be thought as the driver's behavioral fingerprint.

2.4 Introduction of characterised driving behaviours in microsimulation

The last step is to propose a methodology to demonstrate that an observed driving behaviour based on the $p_{IDS,i}$, can be stochastically reproduced in microsimulation for the corresponding driver (reverse problem). This step paves the way for more accurate driver behaviour reproduction and sets the ground for integration in traffic simulation software.

The goal here is to incorporate the PDFs in a car-following model. We simulate an acceleration event with a given duration, desired speed and starting speed, assuming a behaviour described by the specified $p_{IDS,i}$. To achieve this, an ids value is randomly sampled from a specified percentile of the $p_{IDS,i}$. This ids value corresponds to an event of a driver. As a next step, we transform Eq.5 to derive instantaneous ds values, as follows:

$$ds_t = ids_{i,j} \cdot (f_{max}(v_t) - f_{min}(v_t)) + f_{min}(v_t) \quad (7)$$

From Eq.7, we see that a single ids value is sampled from the PDF for the whole duration of an event. This is based on the assumption that the behavior of a driver does not change within a single acceleration event. However, one could sample a different ids value at each time step.

Finally, one can easily extract instantaneous acceleration as follows (based on Eq.3):

$$a_t = [ds_t \cdot (f_{max}(v_t) - f_{min}(v_t)) + f_{min}(v_t)] a_{cp}(v_t) \quad (8)$$

Equations in the form of Eq.7 or Eq.8 can be easily implemented to simulate the free flow speed of a car-following model in microsimulation frameworks.

3. Application

The proposed methodological approach was validated on empirically observed vehicles trajectories. This section first describes the case study. A dataset of multiple drivers under different driving conditions is developed. On the basis of their behaviour, the available pool of drivers is clustered in three main driver types, i.e. timid, normal and dynamic. To efficiently tackle this task this section introduces a discussion and analysis of the inter-driver and intra-driver heterogeneity. The last part of this section refers to the validation of the proposed methodology in terms of driver characterisation and driving style reproduction in simulation.

3.1 Case study

A dataset was created from individual trajectories of 20 drivers collected over a period of 12 months. The vehicle used in the test campaign is a 2.0L diesel C-segment passenger car, equipped with automatic transmission (9 gears), leased for 12 months (second half of 2016 and the first half of 2017). Table 1 summarises the main characteristics of the vehicle.

Table 1. Vehicle's characteristics.

Vehicle category	M1
Model year	2016
Emission standard	Euro6b
Engine capacity	1956 cm ³
Max Power	103 kW
Transmission	Automatic (9 gears)
Fuel type	Diesel
Propulsion type	ICE
Top speed	190 km/h

3.1.1 Campaign

The database of driving data is available at the Joint Research Centre of the European Commission, consisting of more than 10.000 km driven by 20 drivers using the same vehicle. For additional information on the test campaign, the reader can also refer to Pavlovic et al. (2018).

During the period of the experimental campaign, every two weeks, the vehicle was assigned to a volunteer driver, who was free to use it as a personal vehicle without any restriction on the frequency of usage, the driving style, the fuel consumption or the route choice. Fuel was not provided to the volunteer drivers so that the driving style is not influenced. Driving data include trips with different origins and destinations and under different environmental conditions. The dataset covers the most common driving conditions (urban, rural, motorway, and mixed) with a higher occurrence of rural driving conditions due to the local area's characteristics.

Figure 6 illustrates the map of the on-road collected data along with some basic statistics of the experiment and an average per trip speed histogram connected to all drivers.

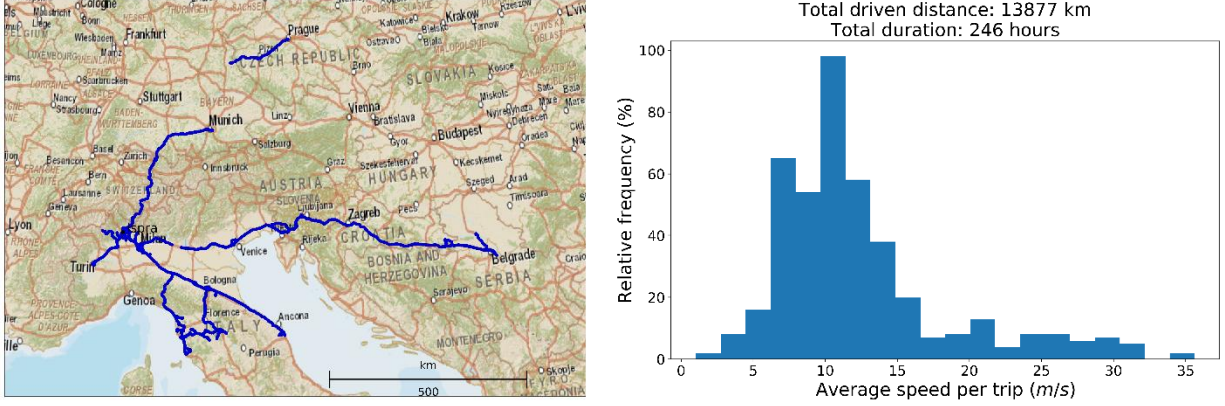


Figure 6. Summary information on the test campaign. The chart on the left shows the area where the experimental campaign was conducted with an indication of the main routes driven. On the right information on the experiment's basic statistics are shown.

3.1.2 Data acquisition and post-processing

Data acquisition was performed with a combination of CAN and On-Board Diagnostics (OBD) II ad-hoc developed to access all the available information from the vehicle. OBD usually provides measurement frequency on average of about 2-4 Hz. With the use of this OBD-CAN logging device, data were recorded at a sampling rate of about 100 Hz. The dataset was post-processed to filter out outliers and set the frequency to 10 Hz. Speed (km/h), Time (s) and Engine Speed (rpm) are the logger signals used in this study.

In the methodology section, for the identification of ds_t , the acceleration potential of the vehicle at a given speed and gear is used. To calculate this variable, one needs to know the speed and gear at each time step as well as the vehicle's maximum power curve. The speed is known from the database. The current gear, though, was not an available piece of information from the experimental measurements. Therefore, to generate accurate estimations, the gear identification algorithm incorporated in the CO2MPAS model (Fontaras et al., 2018) was used. The algorithm estimates the current gear, by finding the closest agreement between the theoretical velocity speed ratio (vsr_{th}) and the experimental velocity-speed ratios (vsr_{exp}) which are calculated according to the formulas mentioned in Eq. 9. For a more detailed description the reader can refer to (Fontaras et al., 2018).

$$vsr_{th} = \frac{2 \cdot \pi \cdot r_d \cdot 3.6}{60 \cdot R_i \cdot gr_i} \left[\frac{km}{h \cdot RPM} \right] \quad (9)$$

$$vsr_{exp} = \frac{v(t)}{N(t)} \left[\frac{km}{h \cdot RPM} \right]$$

where R_i is the final drive ratio for the i^{th} gear, r_d is the dynamic radius of the wheel and gr_i is the i^{th} gear ratio, $v(t)$ is the vehicle's speed at time t and $N(t)$ represents the revolutions per minute in the vehicle's crankshaft at time t .

To retrieve the function of the maximum possible acceleration over speed described in Section 3.2, in this study, the Microsimulation Free-Flow aCceleration model (MFC) (Makridis et al., 2019) is used. It should be noted here that any other vehicle-dynamics-based model can also be used. MFC is a free-flow acceleration model for microsimulation of the vehicle dynamics and the driving style. A publicly available implementation of the model can be found online (<https://pypi.org/project/co2mpas-driver/>). The original model has been designed for Internal Combustion Engine vehicles, yet, an extension of the model for electric powertrains has recently become available (He et al., 2020). The model takes as input common static individual vehicle characteristics (gear ratio, mass, etc.), which can be easily found online, and then estimates the power curves of the vehicle per gear and thus the acceleration potential. Practically, MFC

creates a map function between speed and acceleration and the operational acceleration domain for a specific vehicle. For additional information, we refer the reader to the corresponding publications of the model.

3.1.4 Detection of free-flow acceleration events in the dataset

Here an overview of the detected acceleration events is presented. Table 2 provides an overview of the dataset with distance and trips' time duration per driver. From the total number of events, almost 47.4 % were selected as free-flow. Time duration refers to actual driving time without long pauses. The differences in the number of driven kilometres or hours travelled can be explained by the fact that there was no restriction or guidance on how each driver uses the vehicle. Additionally, this table shows the number of acceleration events detected for each driver along with the distance in km covered during those events.

Table 2. Basic statistics of the trips per driver.

Driver	Total kms	Total hours	Free-flow events number	Events (km)	Driver	Total kms	Total hours	Free-flow events number	Events (km)
D1	250	8	715	117	D11	1056	14	420	171
D2	669	9	447	129	D12	119	4	456	55
D3	1973	39	2807	538	D13	1039	21	1401	307
D4	300	4	223	46	D14	1189	20	1009	295
D5	1055	14	482	134	D15	311	8	548	122
D6	45	2	176	20	D16	2581	35	942	405
D7	166	3	151	58	D17	288	7	632	118
D8	442	13	1054	150	D18	183	7	614	77
D9	310	7	619	111	D19	303	6	345	68
D10	174	6	481	71	D20	1424	19	1139	297

3.2 Assessment, validation and simulation

3.2.1 Deriving continuous distributions from measured events

The fitting outcomes are assessed using the Kolmogorov-Smirnov (K-S) test ("Kolmogorov-Smirnov Test," 2008), which is a nonparametric statistical test of the equality of one-dimensional probability distributions. K-S is used here as a goodness of fit test to compare the observed sample distribution with the continuous reference-fitted probability distribution. The test provides, as a result, the K-S statistic test D and the p -value. The null hypothesis, in this case, is that the two distributions are identical. The hypothesis is rejected if the test statistic D is greater than a critical value obtained for the specific sample size and with a significance level of 1%.

3.2.2 Inter-driver heterogeneity and drivers' clustering

With inter-driver heterogeneity, we refer to the difference in the driving styles among drivers. This heterogeneity is explored through the fitted PDF related to each driver.

The first step to assess the differences among drivers is the visual inspection of the plotted PDFs. From this, a first discrimination among drivers can be made, and a number of different groups of drivers can be inferred. At a second step, after having visually identified 3 groups of drivers, a clustering technique is applied to define the different groups. The well-known K-means algorithm (Macqueen, 1967) is used to cluster the drivers into 3 categories based on a 3D analysis. This clustering technique provides more stable results supposing that the correct number of clusters is chosen (Hsu, 2015). The variables used for the K-means clustering refer to descriptive statistics of the log-normal PDFs. Three features will be used for that, one related to the central tendency of the PDF and another two related to the spread of the PDF (25th, 75th percentiles). The overall result of this stage is the creation of 3 different clusters represented by the specified clustering centres. Those cluster centres represent three different types of drivers, namely a timid, a normal and a dynamic one.

To assess the clustering outcome, we use the two-sample K-S test. This is used initially to test whether two samples come from the same distribution, and the procedure is quite similar to the K-S test mentioned above. In this case, we use the two-sample K-S test to compare the PDFs of drivers in pairs. We generated a sample of 1.000.000 random values based on the PDF of each driver. The null hypothesis, in this case, is that the two samples come from the same distribution. The hypothesis is rejected if the test statistic D is more significant than a critical value obtained for the specific sample size and with a significance level of 1%. In our case, we know a priori that each pair of samples comes from different distributions, which was also confirmed by the test. The goal, however, is to assess how different the two distributions are. The resulting test statistic D indicates the maximum difference between the two cumulative density functions under consideration and this is the indicator used to compare the drivers' PDFs.

3.2.3 Intra-driver heterogeneity

Intra-driver heterogeneity refers to the different driving styles that a driver expresses within a time period and under various conditions. This kind of heterogeneity is assessed here since it is a crucial factor potentially affecting the observed variation in traffic related variables such as headway (Li et al., 2020).

An idea of the variation on the driving style of a single driver, is already taken by observing the fitted PDF. Its wideness visually shows which driver is more consistent to her driving style with respect to others. To explore the intra-driver heterogeneity quantitatively, we refer again to descriptive statistics. More specifically, we use a measure of statistical dispersion, the interquartile range (IQR), which is equal to the difference between 75th and 25th percentiles. Drivers with bigger IQR are considered to have a bigger degree of intra-driver heterogeneity. This heterogeneity is connected to the different driving conditions since the vehicle remains the same in all cases. Evidence for that is provided by comparing the variability of median acceleration of acceleration events among drivers always referring to similar median speed conditions. Drivers with bigger intra-driver heterogeneity are expected to have on average a more variable spectrum of median accelerations with respect to others.

3.2.4 Drivers' behaviour reproduction

Behaviour reproduction is implemented and demonstrated in two levels of detail, the aggregated and the instantaneous one. In this study, the tool used to simulate different driving behaviors related to free-flow state microscopically is the vehicle-dynamics-based MFC. As model input parameters, the following values are used:

- desired speed as the maximum speed of the event,
- starting speed as the minimum speed of the event.
- DS which was not a fixed value as usual for the MFC. For our simulations, ds changed over time as described by Eq. 7 in the methodology section.

It is important to note that any other CF model could be used instead, such as the one developed by Fadloun and Rakha (Fadhloun and Rakha, 2020) and substitute where necessary the acceleration term with Eq. 8.

Firstly, the accuracy of the methodology is tested on a higher level. All the events from all drivers are taken into consideration and simulated. Each event is simulated based on a randomly sampled ids value from the respective PDF $p_{IDS,i}$ of each driver. Due to the stochasticity involved, ten simulations are performed per event. To verify the results, simulated and experimentally measured data are compared with regard to their median acceleration and median speed distributions.

Secondly, the comparison of measured versus simulated values is performed on a micro-level. More specifically, the goal is to observe how accurately the simulation of events describes the instantaneous speed-time drivers' data. For each event, two simulations are implemented, one considering an ids_t value equal to the 25th percentile of the respective PDF $p_{IDS,i}$ and another one corresponding to the 75th percentile. Thereby, an area in the speed-time space is defined bounded by two curves related to the respective

percentiles. This area serves as an area of interest that will denote whether the instantaneous simulations of an event can capture the instantaneous experimental measurements. For demonstrational purposes, such an agreement is presented for a random event of each driver.

3.2.5 Demonstration of simulations of the three driver types

As an outcome of the clustering technique, three different groups of drivers were identified, representing three different kinds of drivers, a timid, a normal and a dynamic one. At this stage, the aim is to showcase through simulations how each type of driver would behave. The nature of the results of such a process is stochastic since the simulation per driver type will be performed considering a randomly selected ids_t value from the respective characteristic per driver PDF $p_{IDS,i}$. Therefore, 1000 simulations per driver type are performed for the defined event. Firstly, we check from an aggregated perspective the median acceleration and median speed distributions of the three types of drivers. Secondly, from a micro perspective, we observe some basic cases of speed-time data connected to the three types of drivers, and we finally present statistics regarding the drivers' performances.

4 Results

The presentation of the results follows the validation workflow described in Section 4.2. First we present the derived continuous PDFs $p_{IDS,i}$ related to each driver, along with the validation results of the fitting process. Afterwards, based on the derived PDFs, the inter-driver heterogeneity is explored and the final 3 groups of drivers are presented along with the results of the 2 sample K-S test which support the creation of the resulting groups. Following that, intra-driver heterogeneity is studied based on each driver's IQR of the respective $p_{IDS,i}$. Finally, the potentials of incorporating the resulting PDFs $p_{IDS,i}$ is demonstrated and taking as an example a hypothetical acceleration event, the performance of each different driver group (dynamic, normal, timid) is assessed.

4.1 Deriving continuous distributions from empirically-derived metric

In the methodology section, $ids_{i,j}$ was identified as a normalised and independent of the speed and the vehicle's powertrain metric necessary to perform an objective comparison between different drivers. In Figure 7, the $ids_{i,j}$ empirical distributions per driver are presented with the y-axis denoting probability density. A three-parameter lognormal PDF $p_{IDS,i}$ (Singh, 1998) is fitted at each one of them and shown as a black curve in the figure. The first parameter (shape) denotes the general form-shape of the distribution and is also equal to the standard deviation of the $\ln(ids_{i,j} - location)$, the second one (location) reveals the shift on the x-axis, representing a lower bound and the last one if combined with the shift parameter (scale + location) expresses the median of the $p_{IDS,i}$. For completion, Appendix C includes the parameters of the inferred $p_{IDS,i}$ s. The location of the median for each $p_{IDS,i}$ is denoted with a vertical red line in the figure.

Table 3 shows the results of the goodness of fit K-S test of all the $p_{IDS,i}$ functions. In all driver cases, the test statistic value was smaller than the critical value ($D < Critical$) which allows us not to reject the null hypothesis and accept, with a 1% level of significance, that all $ids_{i,j}$ distributions can be represented by the inferred $p_{IDS,i}$ s. Additionally, the resulting p-values were larger than the significance level (p-values \gg significance level), providing more evidence on not rejecting the null hypothesis.

The lognormal distribution has been indeed mentioned in the literature as suitable for the description of human behaviors. Gualandi and Toscani studied the connection between human behavior and lognormal distribution also considering cases of modelling drivers in traffic (Gualandi and Toscani, 2019). Regarding transportation research, Antoniou et al. (Antoniou et al., 2002) concluded that the aggregation of traffic measurements forms a statistical distribution, which is quite accurately described by a log-normal distribution.

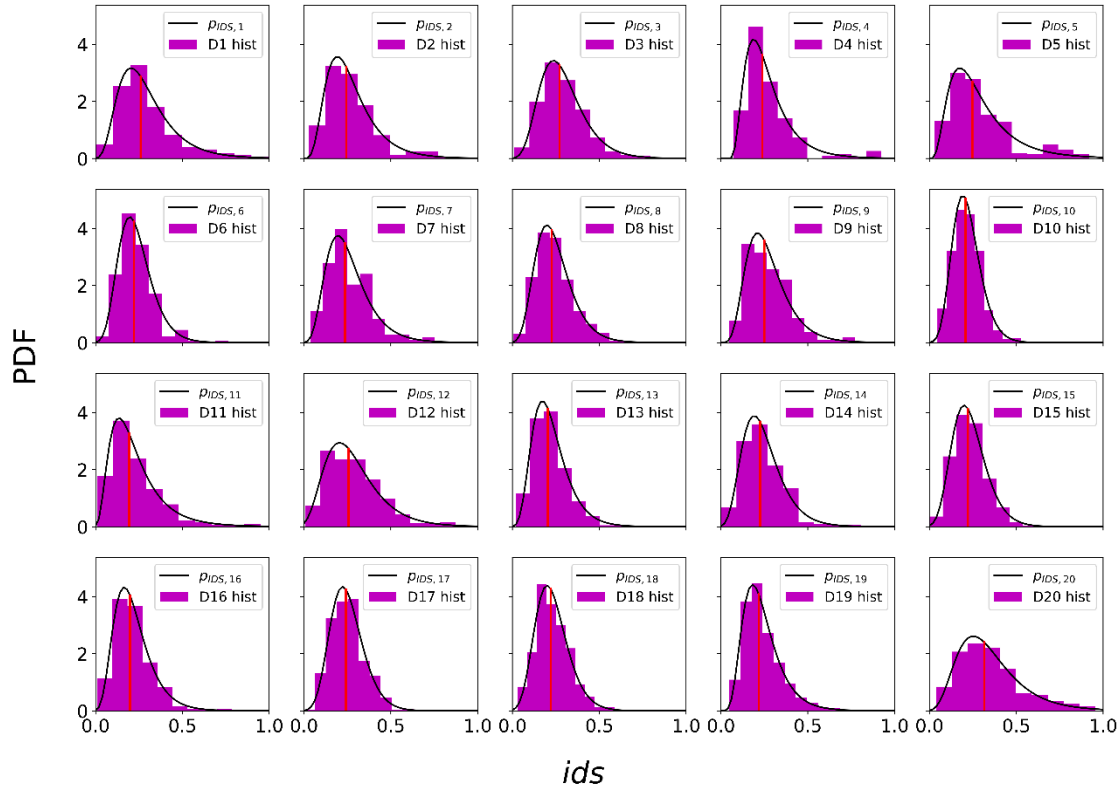


Figure 7. Histogram of the ids values for each driver along with the fitted lognormal probability density function. The vertical red lines denote the location of the median.

Table 3. The goodness of fit test results based on the K-S method.

Driver	Critical value	D statistic	p-value	Driver	Critical value	D statistic	p-value
D1	0.061	0.037	0.280	D11	0.080	0.019	0.999
D2	0.077	0.032	0.739	D12	0.076	0.036	0.596
D3	0.031	0.013	0.710	D13	0.043	0.019	0.662
D4	0.109	0.042	0.822	D14	0.051	0.032	0.264
D5	0.074	0.040	0.404	D15	0.070	0.023	0.928
D6	0.123	0.067	0.391	D16	0.053	0.035	0.188
D7	0.132	0.048	0.870	D17	0.065	0.026	0.768
D8	0.050	0.015	0.969	D18	0.066	0.024	0.859
D9	0.065	0.036	0.396	D19	0.088	0.035	0.782
D10	0.074	0.039	0.435	D20	0.048	0.022	0.662

4.2 Inter-driver heterogeneity and drivers' clustering

A first comparison of the different driving behaviours is showed in Figure 7. A general observation is that drivers do not seem to have tremendous differences. However, there are discrepancies among them, mostly related to the spread of the distribution and less to the location of the median value (red line in the plots). Discrepancies are also seen if one observes the area each $p_{IDS,i}$ covers towards $ids_{i,j}$ values bigger than 0.5. Table 4 provides the median and the 85th percentile values of the $p_{IDS,i}$ s of the drivers. Here we see that the differences among drivers are more prominent in the 85th percentile compared to the medians with the range (larger minus smaller value) of the former being ~ 0.22 , while of the later ~ 0.12 . This implies that the drivers

have not prominently different driving styles when studying them from an aggregated point of view and under real conditions, but they can reveal their differences in specific moments.

Table 4. Median and 85th percentile values of the inferred PDFs

Driver	median	85 th percentile	Driver	median	85 th percentile
D1	0.260	0.444	D11	0.194	0.366
D2	0.242	0.406	D12	0.256	0.442
D3	0.272	0.421	D13	0.204	0.325
D4	0.238	0.390	D14	0.225	0.360
D5	0.247	0.457	D15	0.222	0.336
D6	0.221	0.333	D16	0.199	0.324
D7	0.235	0.381	D17	0.241	0.350
D8	0.227	0.350	D18	0.220	0.329
D9	0.250	0.391	D19	0.218	0.343
D10	0.208	0.300	D20	0.315	0.529

After a more detailed visual inspection of all $p_{IDS,i}$ s taking also into account the median, the 25th and the 75th percentile, drivers are finally heuristically categorised into three different groups. This number was chosen under the following argumentation: Drivers' $p_{IDS,i}$ s belonging in a single group should be quite similar, however, at the same time, the resulting groups should not be very similar to each other; in other words, our goal was to minimise intra-cluster and maximise inter-cluster variation. The goal is that three distinct driving style groups are defined in terms of driving dynamicity. At a second step, a clustering algorithm, namely K-means is applied as an accurate method to group drivers. Figure 8 (a) presents the results of this grouping in the form of a 3D plot. The axes refer to the median, the 25th and the 75th percentile values. Drivers belonging to the same group are plotted with the same marker, while black points show the clustering centers which are the representatives of each group. It is noted that those results were almost identical when selecting the median, the 15th and the 85th percentile values as entry variables instead of the 25th and 75th percentiles. One driver (D20) exhibited more significant differences to the rest of the drivers, which was also obvious in the visual inspection and constituted a separate group.

From the cluster centres, three types of drivers are deducted, a timid (cluster with triangular marker), a normal (cluster with round marker) and a more dynamic one (cluster with rombo marker). The $p_{IDS,i}$ of each driver type is assigned with three percentiles, however, it is identified through its three parameters (shape, location, scale). With the three quantiles known, one can analytically define the three parameters and infer the $p_{IDS,i}$. This procedure is described in detail in Appendix D. Appendix E also reports the inferred parameters of the cluster centers. The $p_{IDS,i}$ s of these driver categories are presented in Figure 8 (b). This figure suggests that differences among different types of drivers are not so big that completely differentiate one driver type from another. The discrimination among them is clear though, in terms of the location of the mode (and consequently the median) as well as the range of values they cover. Timid drivers have ids concentrated more towards smaller values, and their distributions are also less wide, which means that they do not alter a lot their driving behaviour. While dynamic drivers cover a broader spectrum of ids values reaching at some moments quite higher values compared to all others. Therefore, one would expect to identify some drivers as more dynamic than others if big enough data are available. If the number of data is small, the differentiation might be difficult.

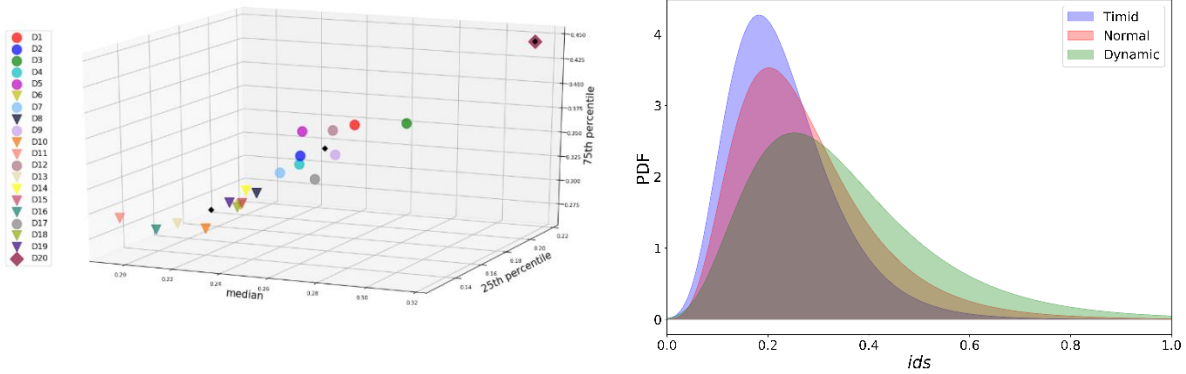


Figure 8. a) K-means clustering result presented in a 3D plot, b) PDFs of the inferred timid, normal and dynamic driver type.

The last step in this section concerns the comparison of drivers in pairs using the two-sample K-S test (Figure 9). This process is used as a tool to assess the clustering process. In each comparison, the null hypothesis is rejected, meaning that the two samples come from different distributions and the p-values being smaller than the significance level of 0.01 also support the rejection of the null hypothesis. The D-statistic reported in the color bar of Figure 10, as mentioned in the methodology, reveals the magnitude of differences among drivers' Cumulative Distribution Functions; hence the smaller it is, the more similar the driving behaviours are. Colour-wise speaking, the closer to purple, the more similar driving behaviours are. Additionally, annotations in the heat map reveal the k-means clustering results with n, t, referring to normal, timid driver group and x the fact that the compared pair of drivers were not assigned to the same group (keeping in mind that D20 constitutes the dynamic group).

As one can see from Figure 9, D20 is indeed quite different from all the others and these differences are the most prominent ones compared to all the other pair comparisons. D20 is only more similar to D1, D3, D5, D12, something which can also be seen in Figure 8 (a). However, taking as an example the pair of D20-D12, their differences even if relatively small, are still comparable to many other pairs of drivers such as D1-D8 or D16-D2 who were classified in different groups. The paired comparison supports the results of the clustering. Overall, drivers who are clustered in the same group, have the biggest similarities and this is obvious when looking at the n or t annotated boxes which have in principle more purplish color with respect to the x annotated boxes.

There are cases where some drivers belonging to one group have the same degree of similarity with others belonging to other groups. An example is D8-D7 and D8-D16, with D8 being in the same cluster with D16 and in a different cluster from D7. These cases refer to drivers who are located in the edges of their cluster and either have many similarities to drivers from other neighbouring clusters or have not so many similarities with drivers of the same cluster who are located in another edge of the same cluster, as can be seen from Figure 8 (a).

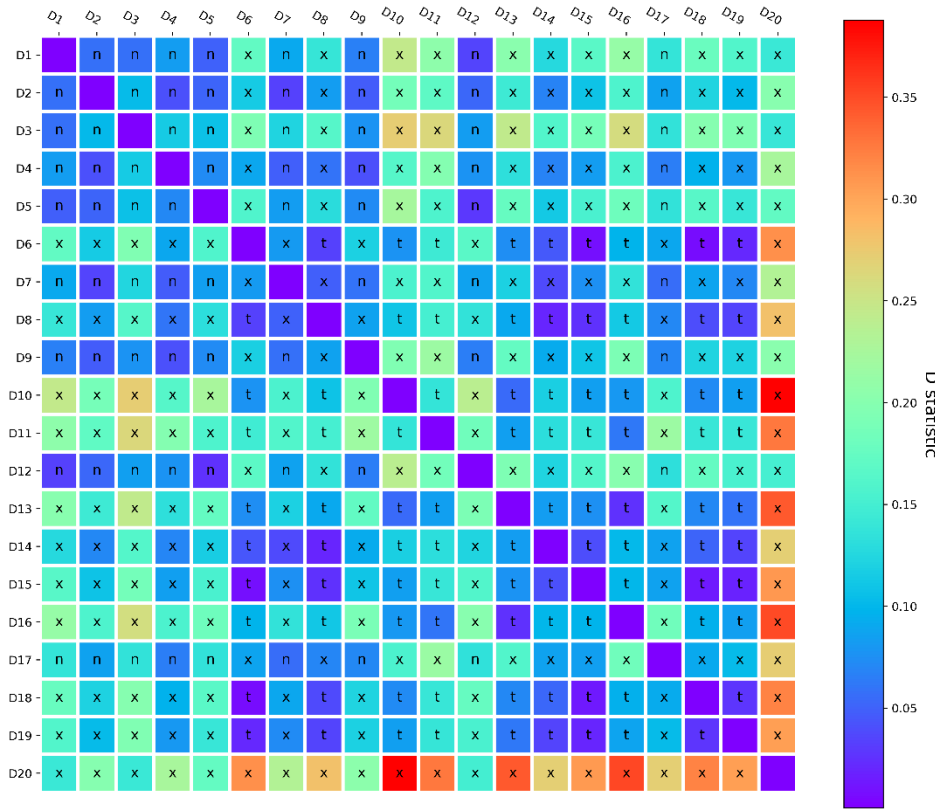


Figure 9. Result of the two-sample K-S test in the form of a heat map.

To provide more evidence-based on the empirical measurements, Figure 10 shows a stacked bar chart denoting the 85th of the median accelerations of the acceleration events of each driver grouped in speed groups of 1 *m/s* range. The 85th percentile is chosen since the differences among drivers are more prominent on specific moments, as mentioned before. On the x-axis one can see the median speed of the events, events for instance, with a median speed of between 4.5 and 5.5 *m/s* were grouped and are represented by the first stacked bar on the left. A median speed range of 5-15 *m/s* is presented, with the criterion that at each speed group, an adequate number of events per driver is assigned. The different drivers are denoted with different colors, 6 drivers are shown, D1, D3, D20, who are characterised among the most dynamic ones as seen from Figure 8 (a) and D10, D11 and D16 as among the timidest ones. It is easily observed that the more dynamic drivers have quite bigger percentile values of their event-related median accelerations for each speed group with respect to the timidest ones. Therefore, the empirically observed measurements support the resulting driver characteristic PDFs.

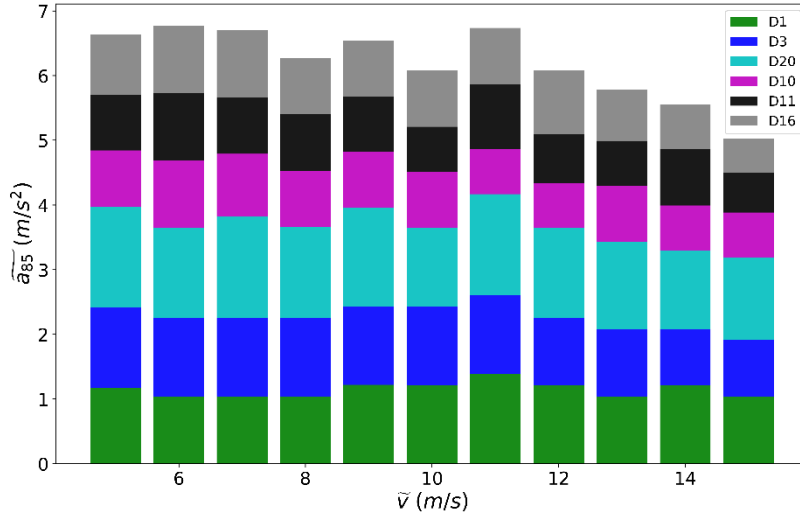


Figure 10. Stacked bar plot of the 85th percentile of median accelerations of events grouped in several speed groups.

4.3 Evidence on intra-driver heterogeneity

By looking at Figure 7, one can observe that some $p_{IDS,i}$ s are wider than others. This implies that their driving behaviour is rather variable. It is important to note that with intra-driver heterogeneity here we refer to the different driving styles a driver expresses under various driving conditions which are bound to the experiment itself. Intra-driver heterogeneity is assessed here through the IQR, the values of which for each driver are illustrated in Figure 11. We suppose that drivers whose PDF has a bigger IQR, exhibit bigger heterogeneity in their own style than others. For instance, D20 who was also ranked as the most dynamic one is also the one with the bigger degree of intra-driver heterogeneity. At the same time D11, who was classified as one of the timider ones, has also a rather variable driving style.

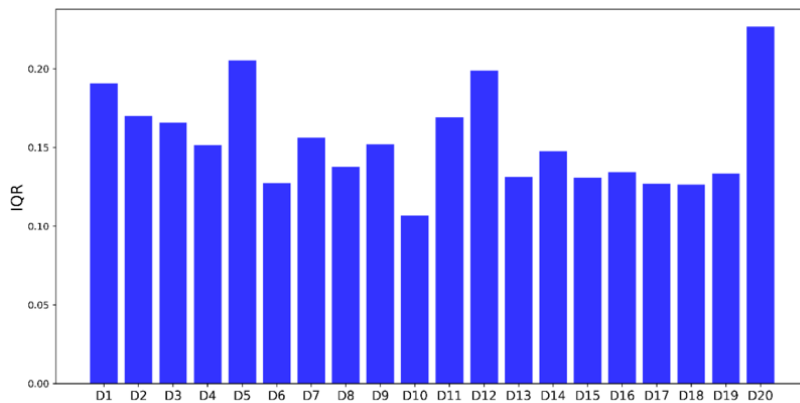


Figure 11. Bar plot of the IQR of the drivers' *IDS* PDFs

To support the concept above, Figure 12 shows a stacked bar chart denoting the IQR of the median accelerations of the acceleration events of each driver grouped in speed groups of 1 m/s range. Here again 6 drivers are shown, D10, D17, D18, who are ranked as the least variable ones as seen from Figure 11 and D5, D12 and D20 as among the most variable. One can see that in most of the speed groups, the drivers ranked as more intra-heterogeneous, exhibit a bigger IQR of the median accelerations of their events.

Especially when comparing D20 and D10 who were ranked as the most and least intra-driver heterogeneous drivers, respectively, they indeed have noteworthy differences in all stacked bars of Figure 12.

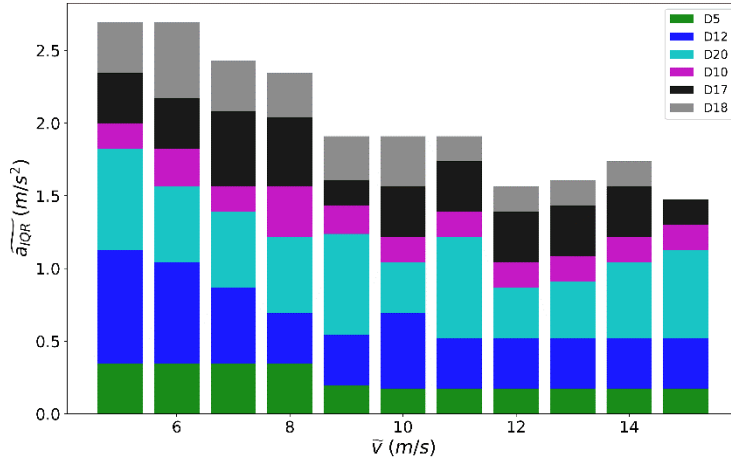


Figure 12. Stacked bar plot of the IQR of median accelerations of events grouped in several speed groups.

5 Implementation in microsimulation

5.1 Drivers' behaviour reproduction

In this section, we test the accuracy of the proposed methodology in respect to driver behavior reproduction in microsimulation. Initially, the test is performed on a macro-level. All acceleration events for each driver were simulated according to the conditions described in methodology and with the variables as described by the respective section in the case study. For each acceleration event, a random ids (ids_r) derived by the respective driver's $p_{IDS,i}$, is considered and by applying Eq.7, ds_t per time step is computed. For statistical purposes, each event is simulated with ten different randomly generated ids_r values. The goal here was to assure that the simulated data are following the experimental ones. Figures 13 and 14 illustrate median acceleration and median speed histograms, both regarding measured data and simulated data. We should remind the reader that acceleration values are quantised, as mentioned earlier in this study, due to the acquiring device, which can affect the empirical data's median acceleration histograms. However, an overall consistency is observed between experimental values and simulations. This means that stochastic simulations of the events based on specific PDFs, in general, represent quite well the specified driver from a macro-perspective which is already sufficient for some cases where a more aggregated view of the acceleration behaviour of drivers is needed.

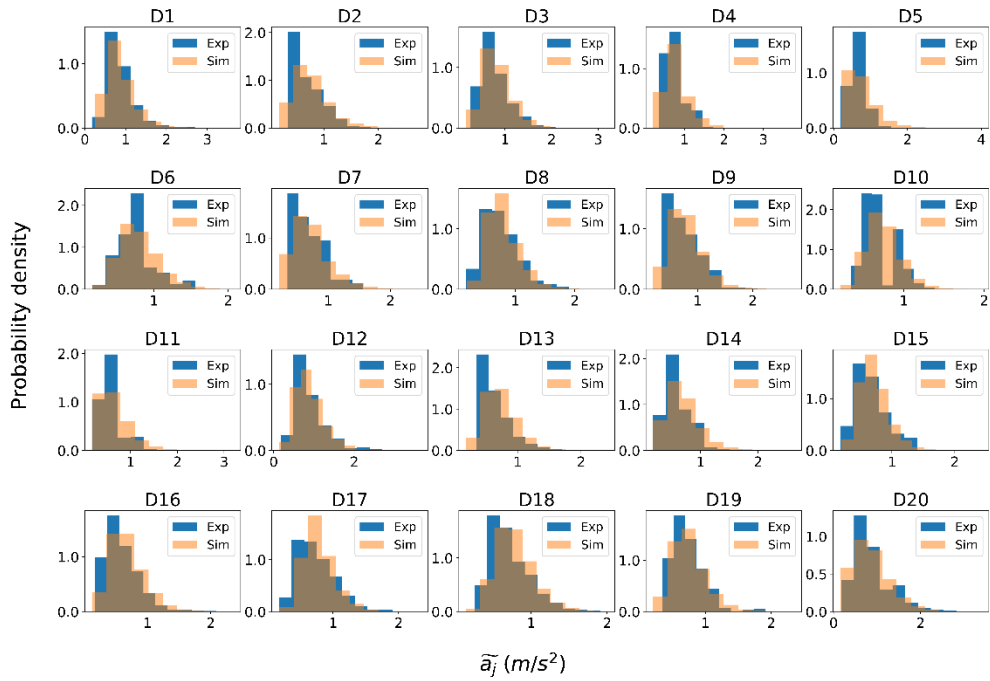


Figure 13. Median acceleration per event histograms of measured and simulated data.

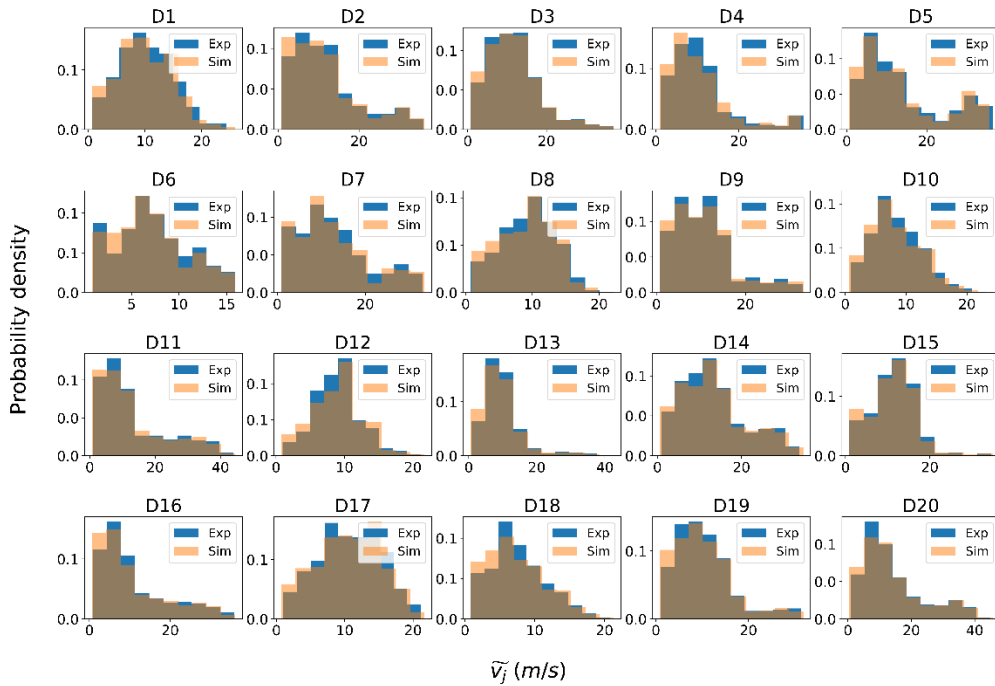


Figure 14. Median speed per event histograms of measured and simulated data.

5.2 Microscopic simulation

In this section, a demonstration of the methodology's potential to contribute to the microsimulation of instantaneous values of acceleration events is presented. Of course, producing stochastic simulations based on a specific driver and comparing them with experimental data of a random event of the respective driver

can provide several results. Therefore, the consistency between simulated and experimental values is not easily determined. To overcome this, we focus on an area of interest for each event which is the area between the simulated curves related to an $ids_{i,j}$ value equal to the 25th and the 75th percentile of the respective $p_{IDS,i}$ as described in the methodology section. This area might be larger or not depending on the driver's variation of her own driving style. Figure 15 demonstrates instantaneous speed versus time values. An event per driver is shown, the black dot points represent the measured values. Two simulations are implemented, the first one considering an ids value of the 25th percentile of the $p_{IDS,i}$ and the second one of the 75th. It can be observed that the experimental measurements lie within the area between the two simulated curves (area of interest). This is important since it indicates the potential of microscopically capturing the acceleration behavior in relation to different drivers.

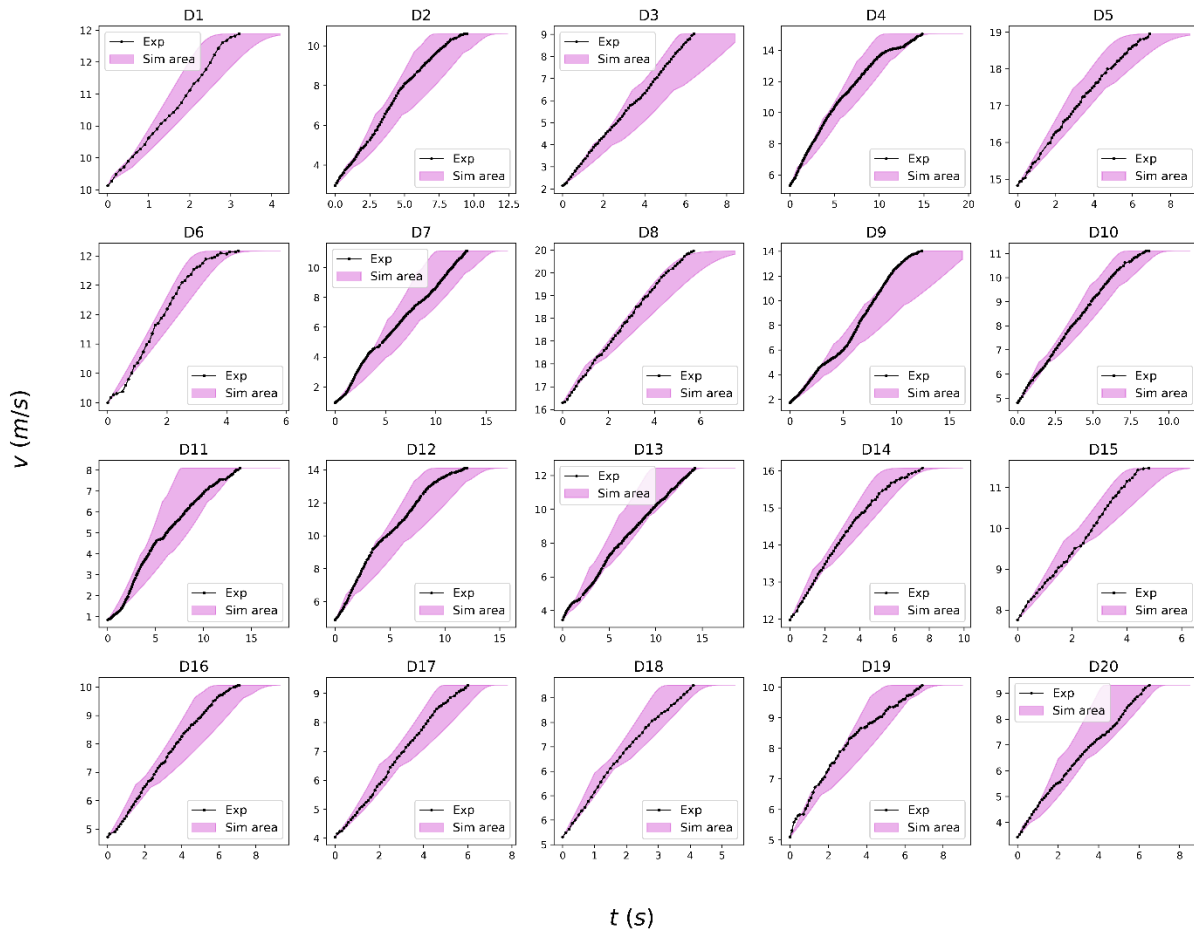


Figure 15. Demo of simulation of instantaneous measurements of speed over time.

5.3 Demonstration of simulations of the three driver types

In this section the differences in the acceleration behaviour of the three driver types, when reproducing an event with the same starting, ending speed and within a given time duration, are presented. The simulated event has the following characteristics, a start speed of 0 m/s , a desired speed of 30 m/s and a duration of 90 seconds. 1000 simulations were performed with randomly selected ids values from the respective PDFs $p_{IDS,i}$ of each driver type. Figure 16 presents the results of this process from a macro-perspective. It shows histograms of median accelerations and median speeds of the simulated event per driver type. One can

distinguish the different types of drivers and as already understood from their log-normal PDFs presented earlier, there are areas of coverage, meaning that the different types of drivers, in general, are not drastically different from each other. We should keep in mind though that here only several simulations of a specific acceleration event are presented.

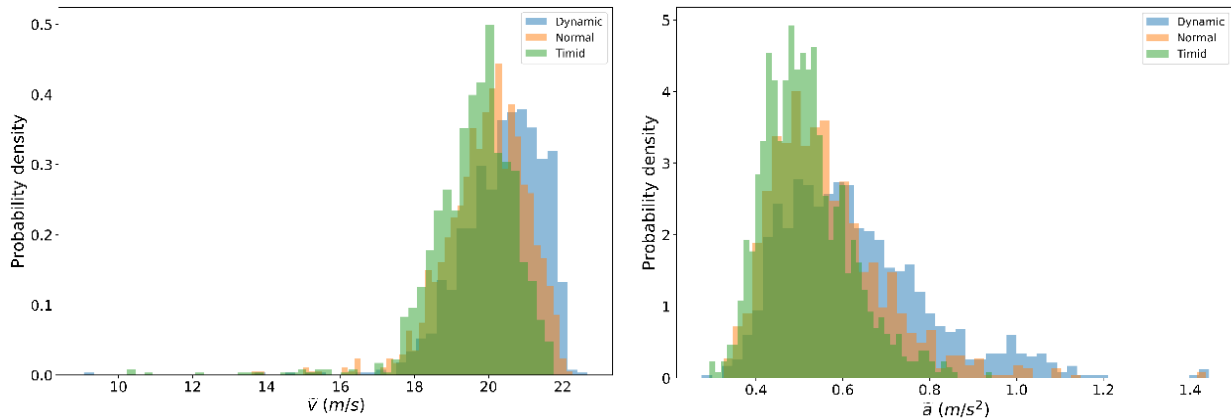


Figure 16. Histograms of median speed and median accelerations of the simulations concerning the three driver types.

Furthermore, Figure 17 presents indicative examples of speed-time evolution of the simulated event as executed by the different driver types. Six different examples are shown, representing the six different observed cases of which driver seemed to have a more abrupt speed change over time. It can be seen, that when stochastic simulations are executed, different outcomes are possible, meaning that a timid driver can have a more aggressive behavior than a normal driver as suggested by the two last plots of Figure 17. To have a more complete overview of the simulated results, Table 5 presents the statistics of the occurrence of each simulation case.

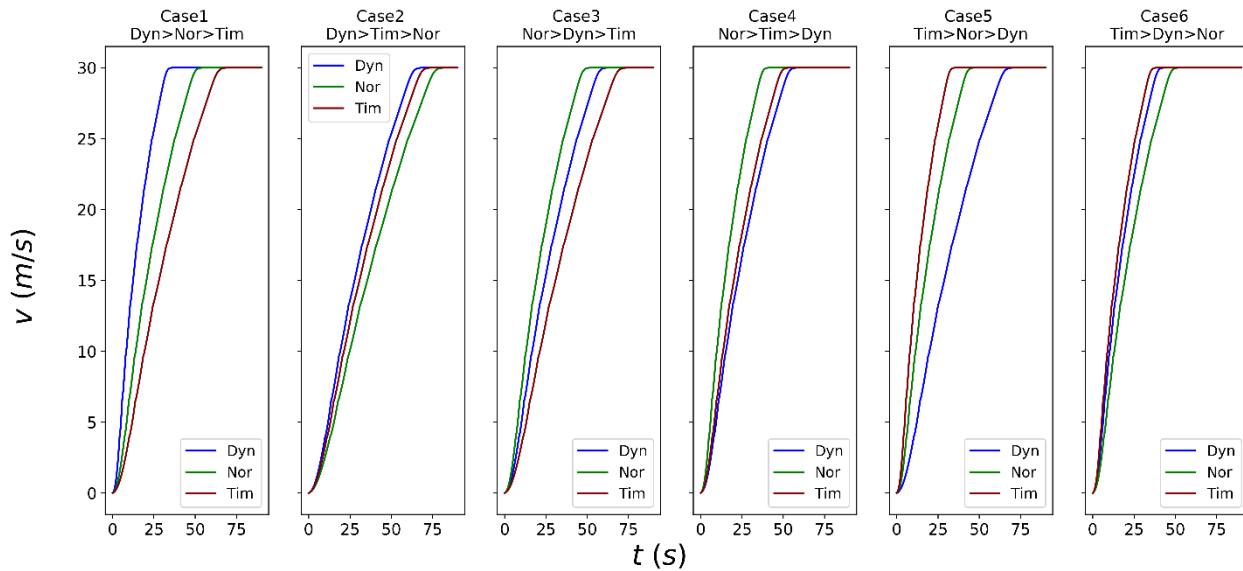


Figure 17. Speed over time plot of the simulated event related to the three driver types. 6 different cases are presented.

Table 5. Percentage of occurrence of each case.

Cases	% of occurrence
1	30.3
2	21.9
3	17.9
4	11.3
5	9.2
6	9.3

6 Conclusion

The present study proposes a comprehensive framework for the characterisation and simulation of drivers' heterogeneity in traffic models. A new metric to identify the driving style independently from the vehicle characteristics and the specific speed is proposed and applied to a database of 20 drivers monitored for about 10.000km over a period of 12 months. Both intra- and inter-driver heterogeneity is studied.

Results showed that log-normal distributions are able to describe the driving style of all drivers. In addition they demonstrated the capability of the methodology to support the proper clusterization of the different drivers and the reproduction of both types of heterogeneity in traffic simulation. This is a very important outcome of the study as the attempts performed so far to use existing modelling framework to incorporate drivers' heterogeneity has provided fairly unsatisfactory results.

In the era of introduction of different types vehicles' automation technologies, the driving behaviour will be one of the key variables in influencing the future traffic dynamics. Having traffic models able to correctly reproduce driving behaviour becomes a fundamental asset to be able to assess the impact of new technologies on the road transportation system.

Acknowledgements

This research has been funded by the Joint Research Centre of the European Commission. The views expressed are purely those of the authors and may not, under any circumstances, be regarded as an official position of the European Commission. The authors are grateful to Vincenzo Arcidiacono for the help regarding CO₂MPAS gear identification tool and to Jelica Pavlovic and Kostis Anagnostopoulos for the help regarding the pre-processing of the experimental data.

References

- Aghabayk, K., Sarvi, M., Young, W., 2015. A State-of-the-Art Review of Car-Following Models with Particular Considerations of Heavy Vehicles. *Transport Reviews* 35, 82–105. <https://doi.org/10.1080/01441647.2014.997323>
- Antoniou, I., Ivanov, V.V., Ivanov, Valery V, Zrellov, P.V., 2002. On the log-normal distribution of network traffic. *Physica D: Nonlinear Phenomena* 167, 72–85. [https://doi.org/10.1016/S0167-2789\(02\)00431-1](https://doi.org/10.1016/S0167-2789(02)00431-1)
- Bokare, P.S., Maurya, A.K., 2017. Acceleration-Deceleration Behaviour of Various Vehicle Types. *Transportation Research Procedia* 25, 4733–4749. <https://doi.org/10.1016/j.trpro.2017.05.486>
- Brooks, R.M., 2012. ACCELERATION CHARACTERISTICS OF VEHICLES IN RURAL PENNSYLVANIA 6.
- Calvert, S.C., van Arem, B., 2020. A generic multi-level framework for microscopic traffic simulation with automated vehicles in mixed traffic. *Transportation Research Part C: Emerging Technologies* 110, 291–311. <https://doi.org/10.1016/j.trc.2019.11.019>
- Chen, D., Ahn, S., Laval, J., Zheng, Z., 2014. On the periodicity of traffic oscillations and capacity drop: The role of driver characteristics. *Transportation Research Part B: Methodological* 59, 117–136. <https://doi.org/10.1016/j.trb.2013.11.005>

- Ciuffo, B., Makridis, M., Toledo, T., Fontaras, G., 2018. Capability of Current Car-Following Models to Reproduce Vehicle Free-Flow Acceleration Dynamics. *IEEE Transactions on Intelligent Transportation Systems* 19, 3594–3603. <https://doi.org/10.1109/TITS.2018.2866271>
- Eboli, L., Mazzulla, G., Pungillo, G., 2016. Combining speed and acceleration to define car users' safe or unsafe driving behaviour. *Transportation Research Part C: Emerging Technologies* 68, 113–125. <https://doi.org/10.1016/j.trc.2016.04.002>
- Fadhloun, K., Rakha, H., 2020. A novel vehicle dynamics and human behavior car-following model: Model development and preliminary testing. *International Journal of Transportation Science and Technology* 9, 14–28. <https://doi.org/10.1016/j.ijtst.2019.05.004>
- Feng, F., Bao, S., Sayer, J.R., Flannagan, C., Manser, M., Wunderlich, R., 2017. Can vehicle longitudinal jerk be used to identify aggressive drivers? An examination using naturalistic driving data. *Accident Analysis & Prevention* 104, 125–136. <https://doi.org/10.1016/j.aap.2017.04.012>
- Fontaras, G., Valverde, V., Arcidiacono, V., Tsiakmakis, S., Anagnostopoulos, K., Komnos, D., Pavlovic, J., Ciuffo, B., 2018. The development and validation of a vehicle simulator for the introduction of Worldwide Harmonized test protocol in the European light duty vehicle CO2 certification process. *Applied Energy* 226, 784–796. <https://doi.org/10.1016/j.apenergy.2018.06.009>
- Gualandi, S., Toscani, G., 2019. Human behavior and lognormal distribution. A kinetic description. *Math. Models Methods Appl. Sci.* 29, 717–753. <https://doi.org/10.1142/S0218202519400049>
- He, Y., Makridis, M., Mattas, K., Fontaras, G., Ciuffo, B., Xu, H., 2020. Introducing Electrified Vehicle Dynamics in Traffic Simulation. *Transportation Research Record* 2674, 776–791. <https://doi.org/10.1177/0361198120931842>
- Hsu, D., 2015. Comparison of integrated clustering methods for accurate and stable prediction of building energy consumption data. *Applied Energy* 160, 153–163. <https://doi.org/10.1016/j.apenergy.2015.08.126>
- Huang, Y.-X., Jiang, R., Zhang, H., Hu, M.-B., Tian, J.-F., Jia, B., Gao, Z.-Y., 2018. Experimental study and modeling of car-following behavior under high speed situation. *Transportation Research Part C: Emerging Technologies* 97, 194–215. <https://doi.org/10.1016/j.trc.2018.10.022>
- Itkonen, T.H., Lehtonen, E., Selpi, 2020. Characterisation of motorway driving style using naturalistic driving data. *Transportation Research Part F: Traffic Psychology and Behaviour* 69, 72–79. <https://doi.org/10.1016/j.trf.2020.01.003>
- James, R.M., Hammit, B.E., 2019. Identifying Contributory Factors to Heterogeneity in Driving Behavior: Clustering and Classification Approach. *Transportation Research Record* 2673, 343–353. <https://doi.org/10.1177/0361198119849404>
- Javanmardi, S., Bideaux, E., Trégouët, J.F., Trigui, R., Tattégrain, H., Bourles, E.N., 2017. Driving Style Modelling for Eco-driving Applications. *IFAC-PapersOnLine* 50, 13866–13871. <https://doi.org/10.1016/j.ifacol.2017.08.2233>
- Jin, X., Zhang, Y., Wang, F., Li, L., Yao, D., Su, Y., Wei, Z., 2009. Departure headways at signalised intersections: A log-normal distribution model approach. *Transportation Research Part C: Emerging Technologies* 17, 318–327. <https://doi.org/10.1016/j.trc.2009.01.003>
- Kessels, F., 2019. *Traffic Flow Modelling: Introduction to Traffic Flow Theory Through a Genealogy of Models*, EURO Advanced Tutorials on Operational Research. Springer International Publishing, Cham. <https://doi.org/10.1007/978-3-319-78695-7>
- Kolmogorov–Smirnov Test, 2008. , in: *The Concise Encyclopedia of Statistics*. Springer New York, New York, NY, pp. 283–287. https://doi.org/10.1007/978-0-387-32833-1_214
- Laval, J.A., Leclercq, L., 2010. A mechanism to describe the formation and propagation of stop-and-go waves in congested freeway traffic. *Phil. Trans. R. Soc. A* 368, 4519–4541. <https://doi.org/10.1098/rsta.2010.0138>
- Laval, J.A., Toth, C.S., Zhou, Y., 2014. A parsimonious model for the formation of oscillations in car-following models. *Transportation Research Part B: Methodological* 70, 228–238. <https://doi.org/10.1016/j.trb.2014.09.004>

- Lee, J., Jang, K., 2019. A framework for evaluating aggressive driving behaviors based on in-vehicle driving records. *Transportation Research Part F: Traffic Psychology and Behaviour* 65, 610–619. <https://doi.org/10.1016/j.trf.2017.11.021>
- Li, G., Li, S.E., Cheng, B., Green, P., 2017. Estimation of driving style in naturalistic highway traffic using maneuver transition probabilities. *Transportation Research Part C: Emerging Technologies* 74, 113–125. <https://doi.org/10.1016/j.trc.2016.11.011>
- Li, L., Fa, W., Rui, J., Jian-Ming, H., Yan, J., 2010. A new car-following model yielding log-normal type headways distributions. *Chinese Phys. B* 19, 020513. <https://doi.org/10.1088/1674-1056/19/2/020513>
- Li, L., Jiang, R., He, Z., Chen, X. (Michael), Zhou, X., 2020. Trajectory data-based traffic flow studies: A revisit. *Transportation Research Part C: Emerging Technologies* 114, 225–240. <https://doi.org/10.1016/j.trc.2020.02.016>
- Macqueen, J., 1967. SOME METHODS FOR CLASSIFICATION AND ANALYSIS OF MULTIVARIATE OBSERVATIONS 5.1, 17.
- Makridis, M., Fontaras, G., Ciuffo, B., Mattas, K., 2019. MFC Free-Flow Model: Introducing Vehicle Dynamics in Microsimulation. *Transportation Research Record* 036119811983851. <https://doi.org/10.1177/0361198119838515>
- Makridis, M., Leclercq, L., Mattas, K., Ciuffo, B., 2020a. The impact of driving homogeneity due to automation and cooperation of vehicles on uphill freeway sections. *Eur. Transp. Res. Rev.* 12, 15. <https://doi.org/10.1186/s12544-020-00407-9>
- Makridis, M., Leclercq, L., Mattas, K., Ciuffo, B., 2020b. Formalising the heterogeneity of the vehicle-driver system to reproduce traffic oscillations. *Transportation Research Part C: Emerging Technologies* 120, 102803. <https://doi.org/10.1016/j.trc.2020.102803>
- Makridis, M., Mattas, K., Anesiadou, A., Ciuffo, B., 2021. OpenACC. An open database of car-following experiments to study the properties of commercial ACC systems. *Transportation Research Part C: Emerging Technologies* 125, 103047. <https://doi.org/10.1016/j.trc.2021.103047>
- Makridis, M., Mattas, K., Ciuffo, B., Re, F., Kriston, A., Minarini, F., Rognelund, G., 2020c. Empirical study on the properties of adaptive cruise control systems and their impact on traffic flow and string stability. *Transp. Res. Rec.* 2674, 471–484. <https://doi.org/10.1177/0361198120911047>
- Makridis, M., Mattas, K., Mogno, C., Ciuffo, B., Fontaras, G., 2020d. The impact of automation and connectivity on traffic flow and CO₂ emissions. A detailed microsimulation study. *Atmos. Environ.* 226, 117399 <https://doi.org/10.1016/j.atmosenv.2020.117399>.
- Mehar, A., Chandra, S., Velmurugan, S., 2013. Speed and Acceleration Characteristics of Different Types of Vehicles on Multi-Lane Highways 13.
- Mei, M., Bullen, A.G.R., n.d. Lognormal Distribution for High Traffic Flows. *TRANSPORTATION RESEARCH RECORD* 4.
- Moridpour, S., 2014. Evaluating the Time Headway Distributions in Congested Highways. *JTLE* 2. <https://doi.org/10.12720/jtle.2.3.224-229>
- Ossen, S., Hoogendoorn, S.P., 2011. Heterogeneity in car-following behavior: Theory and empirics. *Transportation Research Part C: Emerging Technologies* 19, 182–195. <https://doi.org/10.1016/j.trc.2010.05.006>
- Pavlovic, J., Anagnostopoulos, K., Clairotte, M., Arcidiacono, V., Fontaras, G., Rujas, I.P., Morales, V.V., Ciuffo, B., 2018. Dealing with the Gap between Type-Approval and In-Use Light Duty Vehicles Fuel Consumption and CO₂ Emissions: Present Situation and Future Perspective. *Transportation Research Record* 2672, 23–32. <https://doi.org/10.1177/0361198118756894>
- Qi, G., Wu, J., Zhou, Y., Du, Y., Jia, Y., Hounsell, N., Stanton, N.A., 2019. Recognising driving styles based on topic models. *Transportation Research Part D: Transport and Environment* 66, 13–22. <https://doi.org/10.1016/j.trd.2018.05.002>
- Rakha, H., Snare, M., Dion, F., 2004. Vehicle Dynamics Model for Estimating Maximum Light-Duty Vehicle Acceleration Levels. *Transportation Research Record* 1883, 40–49. <https://doi.org/10.3141/1883-05>

- Rakha, H.A., Ahn, K., Faris, W., Moran, K.S., 2012. Simple Vehicle Powertrain Model for Modeling Intelligent Vehicle Applications. *IEEE Trans. Intell. Transport. Syst.* 13, 770–780. <https://doi.org/10.1109/TITS.2012.2188517>
- Saifuzzaman, M., Zheng, Z., Haque, Md.M., Washington, S., 2017. Understanding the mechanism of traffic hysteresis and traffic oscillations through the change in task difficulty level. *Transportation Research Part B: Methodological* 105, 523–538. <https://doi.org/10.1016/j.trb.2017.09.023>
- Singh, V.P., 1998. Three-Parameter Lognormal Distribution, in: *Entropy-Based Parameter Estimation in Hydrology*. Springer Netherlands, Dordrecht, pp. 82–107. https://doi.org/10.1007/978-94-017-1431-0_7
- Spearman, C., 1904. The Proof and Measurement of Association between Two Things. *The American Journal of Psychology* 15, 72–101. <https://doi.org/10.2307/1412159>
- Tanvir, S., 2018. Modeling and Simulation of Driving Activity from an Energy Use-Emissions Perspective.
- Taylor, J., Zhou, X., Roupail, N.M., Porter, R.J., 2015. Method for investigating intradriver heterogeneity using vehicle trajectory data: A Dynamic Time Warping approach. *Transportation Research Part B: Methodological* 73, 59–80. <https://doi.org/10.1016/j.trb.2014.12.009>
- Treiber, M., Kesting, A., 2013. *Traffic Flow Dynamics*. Springer Berlin Heidelberg, Berlin, Heidelberg. <https://doi.org/10.1007/978-3-642-32460-4>
- Wang, W., Xi, J., Zhao, D., 2017. Driving Style Analysis Using Primitive Driving Patterns With Bayesian Nonparametric Approaches. arXiv:1708.08986 [cs].
- Xia, L., Zhu, X., Ma, Z., 2019. Analysis of Driver's Behavior under Following-Go Scenario. Presented at the WCX SAE World Congress Experience. <https://doi.org/10.4271/2019-01-1018>
- Xu, L., Hu, J., Jiang, H., Meng, W., 2015. Establishing Style-Oriented Driver Models by Imitating Human Driving Behaviors. *IEEE Trans. Intell. Transport. Syst.* 16, 2522–2530. <https://doi.org/10.1109/TITS.2015.2409870>
- Yin, S., Li, Z., Zhang, Y., Yao, D., Su, Y., Li, L., 2009. Headway distribution modeling with regard to traffic status, in: *2009 IEEE Intelligent Vehicles Symposium*. Presented at the 2009 IEEE Intelligent Vehicles Symposium (IV), IEEE, Xi'an, China, pp. 1057–1062. <https://doi.org/10.1109/IVS.2009.5164427>
- Zhao, X., Wang, Z., Xu, Z., Wang, Y., Li, X., Qu, X., 2020. Field experiments on longitudinal characteristics of human driver behavior following an autonomous vehicle. *Transportation Research Part C: Emerging Technologies* 114, 205–224. <https://doi.org/10.1016/j.trc.2020.02.018>
- Zheng, Z., Ahn, S., Chen, D., Laval, J., 2011. Freeway traffic oscillations: Microscopic analysis of formations and propagations using Wavelet Transform. *Transportation Research Part B: Methodological* 45, 1378–1388. <https://doi.org/10.1016/j.trb.2011.05.012>
- Zhu, M., Wang, X., Tarko, A., Fang, S., 2018. Modeling car-following behavior on urban expressways in Shanghai: A naturalistic driving study. *Transportation Research Part C: Emerging Technologies* 93, 425–445. <https://doi.org/10.1016/j.trc.2018.06.009>

Appendix

A. Fitted curves defining the operational domain in median *DS*-median Speed space

Table A.1 Characteristics of fitted curves along with the special conditions for each one.

Curve	Polynomial curves	Special conditions
$fmin$	$fmin(\tilde{v}) = 0.009 \cdot \tilde{v} - 0.009$	$fmin(\tilde{v}) \geq Min \widetilde{ds}_{exp}$
$fmax$	$fmax(\tilde{v}) = 3.70 \cdot 10^{-5} \tilde{v}^3 - 0.003 \tilde{v}^2 + 0.084 \cdot \tilde{v} + 0.167$	

Where $Min \widetilde{ds}_{exp}$ is the minimum observed median *ds* value equal to 0.021, \tilde{v} is the median speed value.

B. Relationship of \tilde{a} , \widetilde{ds} and *ids* per event versus \tilde{v}

To showcase the relationship of the \tilde{v}_j , \widetilde{ds}_j and ids_j with \tilde{v}_j with j denoting the event, the Spearman rank-order correlation coefficient (Spearman, 1904) is computed. Spearman correlation is a nonparametric measure of the monotonic relationship between two datasets not necessarily normally distributed. The test provides the spearman correlation coefficient value which lies in the space $[-1,1]$ with 0 implying no correlation. The two-sided p - value is also provided, for a hypothesis test whose null hypothesis is that two sets of data are uncorrelated. In Table B.1, the results of the Spearman rank correlation are presented. In all cases, p - value is zero which denotes the fact that the results are statistically significant and there is much evidence to reject the null hypothesis and consider that in each case the pair of variables compared are correlated. The Spearman correlation values, reveal the evolution from the vehicle dependent and weakly to speed correlated median acceleration feature, to the vehicle independent and strongly correlated to speed \widetilde{ds}_j and finally to the weakly correlated to speed ids_j metric.

Table B.1. Spearman correlation test between median speed - median *ds* and median speed - *ids* per event.

Variables	\tilde{a}_j	\widetilde{ds}_j	ids_j
Spearman Correlation	-0.306	0.818	0.248
\tilde{v}_j p-value. (2-tailed)	0.000	0.000	0.000
N	14651	14651	14651

C. Parameters of the log-normal PDFs of all drivers

Table C.1 presents the lognormal parameters which actually characterise the drivers. One can see that in most cases location parameters are slightly negative which means there is a tiny probability that the PDF takes negative values (more specifically, among all probabilities for an $p_{IDS,i}$ to get values smaller or equal to zero, the biggest one is 0.17%). At this stage we also note that those parameters do mathematically reconstruct each $p_{IDS,i}$, however, they do not directly reveal meaningful information for the log-normal

itself, apart from the location shift. Therefore, descriptive statistics of each $p_{IDS,i}$ are used to analyse further the drivers' characteristics.

Table C.1 Parameters of the log-normal PDFs.

Driver	shape	location	scale	Driver	shape	location	scale
D1	0.448	-0.051	0.311	D11	0.560	-0.025	0.219
D2	0.456	-0.030	0.272	D12	0.383	-0.124	0.381
D3	0.312	-0.120	0.392	D13	0.355	-0.067	0.272
D4	0.529	0.031	0.208	D14	0.334	-0.099	0.324
D5	0.575	-0.011	0.258	D15	0.238	-0.182	0.405
D6	0.265	-0.132	0.353	D16	0.369	-0.068	0.267
D7	0.382	-0.064	0.300	D17	0.207	-0.211	0.452
D8	0.298	-0.113	0.340	D18	0.228	-0.189	0.409
D9	0.378	-0.046	0.295	D19	0.400	-0.026	0.244
D10	0.211	-0.166	0.375	D20	0.410	-0.089	0.405

D. Extracting the three parameters of a log-normal based on three percentiles

In this section, the analytical way of extracting the three parameters of the log-normal PDF (shape, loc, scale) based on its three quantiles (Q_{25}, Q_{50}, Q_{75}) is presented.

Quantile function of a regular log-normal PDF:

$$Quantile = e^{(\mu + \sigma\sqrt{2} \operatorname{erf}^{-1}(2p-1))} \quad D.1$$

For the three parameter log-normal PDF D.1 is slightly transformed as:

$$Quantile = e^{(\mu + \sigma\sqrt{2} \operatorname{erf}^{-1}(2p-1))} + loc \quad D.2$$

Where: $\mu = \ln(\text{scale})$, $\sigma = \text{shape}$, $\operatorname{erf}^{-1} =$ inverse error function, $p =$ the respective percentiles, i.e: 0.25, 0.50, 0.75.

Therefore, by applying D.2, we have the following three equations:

$$Q_{25} = e^{(\mu + \sigma\sqrt{2} \operatorname{erf}^{-1}(2 \cdot 0.25 - 1))} + loc = e^{(\mu + \sigma\sqrt{2} \operatorname{erf}^{-1}(-0.5))} + loc \quad D.3$$

$$Q_{50} = e^{(\mu + \sigma\sqrt{2} \operatorname{erf}^{-1}(2 \cdot 0.5 - 1))} + loc = e^{(\mu + \sigma\sqrt{2} \operatorname{erf}^{-1}(0))} + loc \quad D.4$$

$$Q_{75} = e^{(\mu + \sigma\sqrt{2} \operatorname{erf}^{-1}(2 \cdot 0.75 - 1))} + loc = e^{(\mu + \sigma\sqrt{2} \operatorname{erf}^{-1}(0.5))} + loc \quad D.5$$

Where: $\operatorname{erf}^{-1}(-0.5) = -\operatorname{erf}^{-1}(0.5) \approx -0.477$ and $\operatorname{erf}^{-1}(0) = 0$

Combining D.3, D.4, D.5 and the values of the respective inverse error functions, we have:

$$Q_{25} = e^{(\mu + \sigma\sqrt{2} \operatorname{erf}^{-1}(-0.5))} + loc = e^{(\mu - 0.477\sigma\sqrt{2})} + loc \quad D.6$$

$$Q_{50} = e^{(\mu + \sigma\sqrt{2} \operatorname{erf}^{-1}(0))} + loc = e^{\mu} + loc \rightarrow loc = Q_{50} - e^{\mu} \quad D.7$$

$$Q_{75} = e^{(\mu + \sigma\sqrt{2} \operatorname{erf}^{-1}(2 \cdot 0.75 - 1))} + loc = e^{(\mu + 0.477\sigma\sqrt{2})} + loc \quad D.8$$

Therefore, we have three knowns Q_{25}, Q_{50}, Q_{75} and three unknowns σ, loc, μ .

Combining D.6, D.7 and D.8, we have:

$$e^{(\mu - 0.477\sigma\sqrt{2})} - e^\mu = Q_{25} - Q_{50} \rightarrow e^\mu (e^{(-0.477\sigma\sqrt{2})} - 1) = Q_{25} - Q_{50} \quad \text{D.9}$$

$$e^{(\mu + 0.477\sigma\sqrt{2})} - e^\mu = Q_{75} - Q_{50} \rightarrow e^\mu (e^{(+0.477\sigma\sqrt{2})} - 1) = Q_{75} - Q_{50} \quad \text{D.10}$$

Dividing D9 with D10:

$$\frac{e^{(-0.477\sigma\sqrt{2})} - 1}{e^{(+0.477\sigma\sqrt{2})} - 1} = \frac{Q_{25} - Q_{50}}{Q_{75} - Q_{50}} \quad \text{D.11}$$

We substitute

$$x = e^{(+0.477\sigma\sqrt{2})}, \text{ therefore: } e^{(-0.477\sigma\sqrt{2})} = \frac{1}{x}$$

Also, for convenience we substitute $\frac{Q_{25} - Q_{50}}{Q_{75} - Q_{50}} = c$

Taking these into account, in combination with D11 we end up with:

$$\frac{\frac{1}{x} - 1}{x - 1} = c \rightarrow \frac{1 - x}{x(x - 1)} = c \rightarrow \frac{1 - x}{x(x - 1)} = c \rightarrow cx^2 + (1 - c)x - 1 = 0 \quad \text{D.12}$$

D12 can be easily solved and the solutions are well-known:

$$cx^2 + (1 - c)x - 1 = 0 \rightarrow x = \frac{-(1 - c) \pm \sqrt{(1 - c)^2 - 4c(-1)}}{2c} \rightarrow$$

$$e^{(+0.477\sigma\sqrt{2})} = \frac{-(1 - c) \pm \sqrt{(1 - c)^2 - 4c(-1)}}{2c} \rightarrow$$

$$\sigma = \frac{\ln\left(\frac{-(1 - c) \pm \sqrt{(1 - c)^2 - 4c(-1)}}{2c}\right)}{0.447\sqrt{2}} \quad \text{D.13}$$

D13 provides two possible solutions for σ . To continue with the next unknowns, we subtract D.6 from D.8:

$$Q_{25} - Q_{75} = e^{(\mu - 0.477\sigma\sqrt{2})} + loc - e^{(\mu + 0.477\sigma\sqrt{2})} - loc \rightarrow$$

$$Q_{25} - Q_{75} = e^{(\mu - 0.477\sigma\sqrt{2})} - e^{(\mu + 0.477\sigma\sqrt{2})} = e^\mu (e^{-0.477\sigma\sqrt{2}} - e^{+0.477\sigma\sqrt{2}}) \rightarrow$$

$$e^\mu = \frac{Q_{25} - Q_{75}}{e^{-0.477\sigma\sqrt{2}} - e^{+0.477\sigma\sqrt{2}}} \xrightarrow{e^\mu = scale}$$

$$scale = \frac{Q_{25} - Q_{75}}{e^{-0.477\sigma\sqrt{2}} - e^{+0.477\sigma\sqrt{2}}} \quad \text{D.14}$$

D14 provides two possible solutions for $scale$ since there are two possible solutions for σ .

Finally, from D7 there are also two possible solutions for the loc parameter:

$$loc = Q_{50} - \frac{Q_{25} - Q_{75}}{e^{-0.477\sigma\sqrt{2}} - e^{+0.477\sigma\sqrt{2}}} \quad \text{D.15}$$

After solving the equations numerically, one can easily reject one of the two possible solutions for the derived parameters shape, loc, scale since they provide unrealistic results.

E. Parameters of the log-normal PDFs of the three inferred type of drivers

Table E.1 Parameters of the log-normal PDFs of the different driver types.

Driver type	shape	location	scale
Timid	0.335	-0.081	0.295
Normal	0.416	-0.047	0.296
Dynamic	0.410	-0.089	0.405